



HAL
open science

The phase relationship between the pyrazinamide polymorphs α and γ

Kangli Li, Gabin Gbabode, María Barrio, Josep-Lluis Tamarit, Marine Vergé-Depré, Benoit Robert, Ivo Rietveld

► **To cite this version:**

Kangli Li, Gabin Gbabode, María Barrio, Josep-Lluis Tamarit, Marine Vergé-Depré, et al.. The phase relationship between the pyrazinamide polymorphs α and γ . *International Journal of Pharmaceutics*, 2020, 580, pp.119230. 10.1016/j.ijpharm.2020.119230 . hal-02551771

HAL Id: hal-02551771

<https://normandie-univ.hal.science/hal-02551771>

Submitted on 22 Aug 2022

HAL is a multi-disciplinary open access archive for the deposit and dissemination of scientific research documents, whether they are published or not. The documents may come from teaching and research institutions in France or abroad, or from public or private research centers.

L'archive ouverte pluridisciplinaire **HAL**, est destinée au dépôt et à la diffusion de documents scientifiques de niveau recherche, publiés ou non, émanant des établissements d'enseignement et de recherche français ou étrangers, des laboratoires publics ou privés.



Distributed under a Creative Commons Attribution - NonCommercial 4.0 International License

The phase relationship between the pyrazinamide polymorphs α and γ

Kangli Li¹, Gabin Gbabode¹, Maria Barrio², Josep-Lluís Tamarit², Marine Vergé-Depré³, Benoît Robert³, Ivo B. Rietveld^{1,4,*}

¹ Laboratoire SMS-EA3233, UFR des Sciences et Techniques, Université de Rouen Normandie, Place Emile Blondel, 76821 Mont-Saint-Aignan, France

² Grup de Caracterització de Materials, Departament de Física and Barcelona Research Center in Multiscale Science and Engineering, Universitat Politècnica de Catalunya, EEBE, Campus Diagonal-Besòs, Av. Eduard Maristany 10-14, E-08019 Barcelona, Catalonia, Spain

³ Sanofi R&D, Pharmaceuticals Development Platform/Analytical Sciences/Solid State Group, 13 quai Jules Guesde, F-94400 Vitry sur Seine, France

⁴ Faculté de Pharmacie, Université Paris Descartes, 4 avenue de l'observatoire, 75006 Paris, France

* Corresponding author: ivo.rietveld@univ-rouen.fr

Abstract

Pyrazinamide is an active pharmaceutical compound for the treatment of tuberculosis. It possesses at least four crystalline polymorphs. Polymorphism may cause solubility problems as the case of ritonavir has clearly demonstrated; however, polymorphs also provide opportunities to improve pharmaceutical formulations, in particular if the stable form is not very soluble. The four polymorphs of pyrazinamide constitute a rich system to investigate the usefulness of metastable forms and their stabilization. However, despite the existence of a number of papers on the polymorphism of pyrazinamide, well-defined equilibrium conditions between the polymorphs appear to be lacking. The main objectives of this paper are to establish the temperature and pressure equilibrium conditions between the so-called α and γ polymorphs of pyrazinamide, its liquid phase, and vapor phase and to determine the phase-change inequalities, such as enthalpies, entropies, and volume differences. The equilibrium temperature between α and γ was experimentally found at 392(1) K. Moreover, vapor pressures and solubilities of both phases have been determined, clearly indicating that form α is the more stable form at room temperature. High-pressure thermal analysis and the topological pressure-temperature phase diagram demonstrate that the γ form is stabilized by pressure and becomes stable at room temperature under a pressure of 260 MPa.

KEYWORDS

Vapor pressure, solubility, thermal expansion, solid-solid transition, specific volume, pressure-temperature phase diagram, active pharmaceutical ingredient

1. Introduction

1.1 Crystalline Polymorphism

Polymorphism is an aptitude of organic and inorganic compounds to crystallize in different crystal structures. Intermolecular interactions and free energies will be different for each crystal structure (Hilfiker, 2006). Thus, for applications that depend on consistency and stability, such as drugs, it is important to understand which of the possible forms is the most stable, and how to control the persistence of a formulation for a required amount of time in case the chosen form is not the more stable one. Changes in the crystal structure will affect the solubility and bioavailability of drugs (Censi and Di Martino, 2015), the crystal shape and flowability (Datta and Grant, 2004), and the crystal volume, which may cause formulations such as tablets to disintegrate (Su et al., 2018). Polymorph transformations can occur during storage or during processing like tableting or wet granulation (Brits et al., 2010; Morris et al., 2001). In this paper, the active pharmaceutical ingredient (API) pyrazinamide with at least four polymorphs, α , β , γ , and δ is investigated. The phase behavior of pyrazinamide will be discussed with a focus on the α and γ phases for which we present new data.

1.2 Literature data on the phase behavior of pyrazinamide

Pyrazinamide (PZA) is an API against tuberculosis and its molecular structure is shown in Figure 1. Forms Polymorphs α , β and γ are monoclinic, and their space groups are $P2_1/n$, $P2_1/c$ and Pc , respectively, whereas δ is triclinic and its space group is $P\bar{1}$ (A.Nangia and A.Srinivasulu, 2005; Battilocchio et al., 2014; Castro et al., 2009; Cherukuvada et al., 2010; Jarzemska et al., 2014; Nakata and Takaki, 1987; Rajalakshmi et al., 2014; Rø and Sørum, 1972a, b; Takaki et al., 1960; Tamura et al., 1961; Tiwari et al., 1980; Tiwari et al., 1982). Comparing the packing of the four forms, the α , β and δ forms contain head-to-head hydrogen bonded dimers between the amide groups. In the γ form, the molecules are arranged in catemers with hydrogen bonds linking the amide group with the top of the pyrazine ring. The γ polymorph exhibits disorder in which for about 20 % of the molecules the position of the ring and the amide group are inverted (Cherukuvada et al., 2010; Wahlberg et al., 2013).

Besides the polymorphs, a lot of crystallographic work has been carried out on mixtures of PZA with excipients or other APIs. Cocrystals containing pyrazinamide with carboxylic acids (Abourahma et al., 2015; Adalder et al., 2012; Kulla et al., 2016; Luo and Sun, 2013), with haloperfluorinated compounds (Choquesillo-Lazarte et al., 2017), with hydrochlorothiazide (Wang et al., 2014), with pyrogallol (Thakuria et al., 2012) and with diflunisal (Évora et al., 2011) have been described. Several polymorphs of cocrystals of PZA with succinic acid (Cherukuvada and Nangia, 2012; Luo and Sun, 2013), malonic acid (Kulla et al., 2017) and theophylline (Eddleston et al., 2015) have been found and investigated. Different binary mixtures leading to either cocrystals or eutectic systems have been described by Rajbongshi et al. (Rajbongshi et al., 2018). A ternary cocrystal has been designed by using a “drug-bridge-drug” strategy involving PZA combined with another first-line antitubercular drug isoniazid using fumaric acid as the bridge (Liu et al., 2018).

Calorimetric data available in the literature on the different polymorphs have been compiled in Table 1. The average melting temperature of form γ observed in the literature is 462(2) K¹ with very little variation in the data. The melting enthalpy exhibits a larger spread around the average value of 221(10) J g⁻¹, while the value of 177 J g⁻¹ has been omitted as a clear outlier. The average solid-solid transition temperature observed for α - γ is 421(4) K with an enthalpy of 11(4) J g⁻¹. However, Castro et al. carried out thorough investigations on the phase behavior of PZA using differential scanning calorimetry (DSC) and thermal stage microscopy, supported by X-ray powder diffraction (XRPD) and infrared spectroscopy and they observed that the α - γ transition depends on the heating rate of the DSC (Castro et al., 2009). This makes it rather doubtful that the average observed solid-solid transition temperature between α and γ is their equilibrium temperature. Cherukuvada et al. reported on polymorphic transition temperatures and enthalpies, relative stabilities and crystal structure data (at 100 K) (Cherukuvada et al., 2010). A schematic energy-temperature diagram was established resulting in the following stability hierarchy at room temperature $\alpha > \delta > \gamma > \beta$ with α the thermodynamically stable polymorph (Cherukuvada et al., 2010). Castro et al. reached a similar conclusion with the stability hierarchy of $\delta > \alpha > \gamma$ at low temperature, which may or may not include room temperature (Castro et al., 2009). γ is the stable form at high temperature in all references. The specific volume of different polymorphs of PZA in the literature is shown in Table 2.

Table 1. Calorimetric and crystallographic data of the different phase transitions of pyrazinamide in the literature^a

Transition	T/K	$\Delta H / J g^{-1}$	Heating rate /K min ⁻¹	References
$\gamma \rightarrow L$	461.4(5)	228(5)	10	(Castro et al., 2009)
	461.5(1)	228(3)	10	(E. Castro et al., 2011)
	461.8(2)	213(5)	5	(Cherukuvada et al., 2010)
	462.5(2)	220(5)	2	(Blokhina et al., 2015b)
	462.25	221.6	10	(Wheate et al., 2010)
	465.7(2)	220(5)	2	(Blokhina et al., 2015a)
	463.15		10	(Luo and Sun, 2013)
	461.15	177	10	(Lavor et al., 2012)
	461.4(5)	229(3)	5	(Lourenço et al., 2012)
	462.2(1)		10	(Pajula et al., 2010)
461.5(1)	217(24)	5	(Baaklini et al., 2015)	
	418.15-419.15			(Sharma et al., 2018)
$\alpha \rightarrow \gamma$	420.1(5)	13.2(7)	10	(Castro et al., 2009)
	428.25	10.6	5	(Cherukuvada et al., 2010)
	420.15	5	10	(Lavor et al., 2012)
	420.4(5)	13.3(2)	5	(Lourenço et al., 2012)
	420.65	11.35	5	(Baaklini et al., 2015)
$\delta \rightarrow \gamma$	408(5)	17(2)	10	(Castro et al., 2009)
	404.35	13.5	5	(Cherukuvada et al., 2010)

¹ The number in parentheses is the uncertainty in the last digit of the value, i.e. 1.23(4) equals 1.23 ± 0.04.

$\delta \rightarrow \alpha$	395(1)	$\Delta H > 0^b$	10	(Castro et al., 2009)
$\beta \rightarrow \gamma$	368.15	$\Delta H > 0^b$	10	(Castro et al., 2009)
	372.55	6.3	5	(Cherukuvada et al., 2010)
PZA \rightarrow vap		829(18) ^c		(Ribeiro da Silva et al., 2005)
$\alpha \rightarrow$ vap		915(13) ^d		(Blokhina et al., 2015a)
$\alpha \rightarrow$ vap		715(44) ^e		(Negoro, 1959; Negoro, 1960)

^a Values from the literature reported in °C or in J mol⁻¹ are adjusted by adding 273.15 K or are divided by 123.11 g mol⁻¹, respectively; an average value is used in this table when multiple values have been reported in the same paper; values are rounded to the number of reported digits in the respective reference.

^b Enthalpy values have not been mentioned in the reference (Castro et al., 2009), but DSC curves in the figures indicate endothermic transitions with increasing temperature.

^c Most likely form γ as the temperature of measurement is 421 K, however the enthalpy has been adjusted by the authors to the value expected at 298.15 K.

^d The temperature range is from 359.15 K to 383.15 K.

^e The temperature range is from 353.15 K to 383.15 K.

Table 2. Specific volume of different polymorphs of PZA in the literature

Polymorph	Space group	T/ K	V ^a / Å ³	Specific volume ^b / cm ³ g ⁻¹	References ^c
α	<i>P2₁/a</i>	RT ^d	567.518	0.69403	PYZIN (Takaki et al., 1960)
	<i>P2₁/c</i>	RT ^d	569.817	0.69684	PYZIN04 (Tiwari et al., 1980)
	<i>P2₁/a</i>	RT ^d	577.773	0.70657	PYZIN14 (Tiwari et al., 1982)
	<i>P2₁/n</i>	100	546.642	0.66850	PYZIN15 (A.Nangia and A.Srinivasulu, 2005)
	<i>P2₁/n</i>	180	554.291	0.67785	PYZIN21 (Battilocchio et al., 2014)
	<i>P2₁/n</i>	100	547.276	0.66927	PYZIN22 (Rajalakshmi et al., 2014)
β	<i>P2₁/c</i>	RT ^d	559.730	0.68450	PYZIN01 (Rø and Sørnum, 1972a)
	<i>P2₁/c</i>	90	540.881	0.66145	PYZIN23 (Jarzembska et al., 2014)
	<i>P2₁/c</i>	100	540.354	0.66081	PYZIN18 (Cherukuvada et al., 2010)
δ	<i>P$\bar{1}$</i>	RT ^d	279.557	0.68375	PYZIN02 (Rø and Sørnum, 1972b)

	$P\bar{1}$	100	268.818	0.65749	PYRZIN16 (A.Nangia and A.Srinivasulu, 2005)
	Pa	RT ^d	280.040	0.68493	PYRZIN03 (Tamura et al., 1961)
	Pa	RT ^d	275.136	0.67294	PYRZIN05 (Nakata and Takaki, 1987)
γ	Pc	293	275.917	0.67485	PYRZIN17 (Castro et al., 2009)
	Pc (with disorder) ^e	100	268.057	0.65562	PYRZIN19 (Cherukuvada et al., 2010)
	Pc (without disorder) ^f	100	267.226	0.65359	PYRZIN20 (Cherukuvada et al., 2010)

^aThe data is obtained from the CSD.

^bSpecific volume is calculated with the unit cell volume.

^cCSD reference code and literature reference.

^dRoom temperature: 283-303K.

^e Disorder taken into account.

^f Disorder not taken into account.

Including pressure into the analysis, Tan et al. found crystallographic indications that γ transforms into β at a pressure of about 4 GPa at room temperature (Tan et al., 2012). It implies that form β would be more stable than γ above 4 GPa. For α and δ , no transformations under pressure have been observed up to 13 GPa (Tan et al., 2012). Smets et al. investigated the transformation mechanism of PZA and concluded that the transition from the γ form to the low temperature δ and α forms include a vapor-mediated recrystallization process, while the transition from the low temperature forms to the γ form during heating included nucleation and growth within the crystal (Smets et al., 2018).

Because γ is a metastable form of PZA under ambient conditions, which is easily obtained through processing, it may be an interesting target to increase the bioavailability of PZA, although the polymorph does not persist for a long time under ambient conditions (Baaklini, 2015; Baaklini et al., 2015; Smets et al., 2018). Baaklini et al. have investigated polymorph control by spray drying with different additives and they managed to prevent spontaneous transformation of γ . They also found that the γ form persists at room temperature for several years by co-spray drying with 1,3-dimethylurea (Baaklini, 2015; Baaklini et al., 2015).

Pyrazinamide is prone to crystallize and the vitreous state is very difficult to reach. Borba et al. prepared the vitreous state by depositing vapor at 10 K and they observed recrystallisation into the δ phase at 260 K while heating (Borba et al., 2009), which is the closest observation to a glass transition temperature reported in the literature, if one assumes that PZA crystallizes immediately once it reaches T_g on heating the glass. Cooling crystallization from solution specifically targeting the δ form has been published by Hermanto et al. (Hermanto et al., 2015). Solubility of α , γ and δ in water and solubility of α in

four organic solvents and one mixture of solvents have been determined. The results showed that the solubility of PZA increases with increasing temperature and the solubility data in water from about 287 K to 316 K indicated the following ranking $x(\gamma) > x(\delta) > x(\alpha)$. Solubility of α in various solvents have been obtained by Zhang et al. (Zhang et al., 2017).

A number of modelling studies involving PZA have been published. The most extensive is that of Wahlberg et al. demonstrating and quantifying disorder in the structure of the γ form (Wahlberg et al., 2013) as mentioned before by Cherukuvada et al. (Cherukuvada et al., 2010). Computational studies specifically targeting the β form of pyrazinamide have been published by Jarzemska et al. (Jarzemska et al., 2014). The α - γ phase transformation has been investigated by in situ Raman and density functional theory (DFT) leading to a transition temperature of 418.15-419.15 K (Sharma et al., 2018). The four polymorphs of PZA have been studied by Hirshfeld surface and fingerprint plots (Luo et al., 2015).

A few studies have been published on vapor pressure of PZA. Blokhina et al. provided the vapor pressure as a function of the temperature from 359.15 K to 383.15 K: $\ln(P / \text{Pa}) = -13360(178) / T (\text{/K}) + 38.3(5)$, which was verified to belong to the alpha phase (Blokhina et al., 2015a). Negoro et al. reported the vapor pressure of the α form as a function of temperature from 353.15 K to 383.15 K as well (Negoro, 1960). Ribeiro et al. obtained the vapor pressure of most likely the γ form, considering the measurement temperature, but the authors did not verify the polymorph under study (Ribeiro da Silva et al., 2005). The sublimation enthalpy values from the different vapor pressure measurements vary too much to draw any solid conclusions about the stability and the equilibrium temperature between the α and γ phases (Table 1).

1.3 Topological pressure-temperature phase diagrams

Pressure-temperature (P-T) phase diagrams provide information on the relative stability between crystalline polymorphs as a function of the thermodynamic variables, characteristic for the Gibbs energy function, temperature and pressure. Such phase diagrams can be obtained by direct measurement, but due to experimental limitations, it is often easier to use the Clapeyron equation (eq. 1) to complete the phase diagram (Barrio et al., 2017; Inès et al., 2013):

$$\frac{dP}{dT} = \frac{\Delta S}{\Delta V} = \frac{\Delta H}{T\Delta V} \quad (1)$$

in which, ΔS is the entropy change between the two phases, ΔH is the enthalpy change, ΔV represents the volume change, and T is the equilibrium temperature at which the enthalpy change has been obtained. Eq. 1 provides the slope of a two-phase equilibrium as a function of the temperature and the pressure and phase diagrams obtained through extrapolation are called topological phase diagrams, because the positions of the equilibria will be qualitatively correct, but the uncertainty over their position may be larger than in the case of experimentally obtained equilibrium information.

In this paper, the phase behavior of polymorphs α and γ of pyrazinamide is reported using

data from DSC, PXRD, synchrotron PXRD and High-Pressure Differential Thermal Analysis (HP-DTA). The melting temperature and enthalpy of γ have been reviewed and those of α have been determined. In addition, a thorough study of the α - γ transition temperature and enthalpy has been carried out. Specific volumes as a function of temperature and pressure of these two polymorphs have been obtained by XRPD. The melting equilibrium of γ and the transition between α and γ have been measured by HP-DTA. Finally, the vapor pressure and the solubility of the α and γ forms have been measured. All the data has been combined to build a topological phase diagram demonstrating the stability hierarchy of the two polymorphs as a function of pressure and temperature.

2. Materials and Methods

2.1 Pyrazinamide

Pyrazinamide was purchased from Sigma-Aldrich (France) and its purity is $\geq 97.5\%$ (GC). The commercial form was determined to be polymorph α by X-ray diffraction. Single crystals of α were obtained by sublimation. The γ form was obtained by heating the commercial sample above the α - γ transition temperature (see text), but it can also be obtained from spray drying. PXRD and DSC were used to verify the obtained polymorphs.

2.2 Crystal growth by sublimation

The sublimation experiments have been carried out with a cylindrical oven containing a linear array of six independently controlled heating elements. A glass tube with 0.1 g of PZA was placed in the oven under atmospheric pressure, while the set temperature ranged from 353 K to 403 K (± 0.5 K). Using the independent heating elements, various gradients along the glass tube were imposed. The time for sublimation experiments ranged from 2 days to 2 weeks. No significant decomposition took place during these experiments as confirmed by chromatographic measurements (See Figure S4).

2.3 High-resolution powder X-ray powder diffraction

High-resolution PXRD was used to determine the specific volumes of the α and γ forms as a function of the temperature. Powdered specimens were placed in capillaries of 0.5 mm diameter. The measurements were carried out with a vertically mounted INEL cylindrical position sensitive detector (CPS-120) and by using the Debye–Scherrer geometry. Monochromatic Cu- $K\alpha_1$ radiation (1.54056 Å) applying an asymmetrically focusing incident-beam curved germanium monochromator was used and diffraction intensities were registered over a 2θ range from 3.0° to 111.878° with a step size of 0.029° . The temperature was controlled by a liquid nitrogen 700 series Cryostream Cooler (Oxford Cryosystems). The PXRD patterns were refined by FullProf software to calculate the specific volumes (Rodriguez-Carvajal et al., 2005).

2.4 Synchrotron powder X-ray diffraction

The specific volumes of α and γ as a function of pressure at room temperature were obtained using PXRD data measured on the high-pressure diffraction beamline PSICHE at the synchrotron SOLEIL (Gif sur Yvette, France) using a focused monochromatic mode and a Ge solid state detector. High pressure was controlled with a membrane driven diamond anvil cell

with an upper pressure limit of 2 GPa. Silicon oil was used as pressure transmitting medium. NaCl was used as an internal reference to determine the pressure. The wavelength used for the experiments was 0.4859 Å. Pawley fit refinements were carried out using TOPAS-Academic V4.1 software.

2.5 Differential Scanning Calorimetry

The thermal behavior of PZA was studied by two different calorimeters: a TA Q100 thermal analyzer and a DSC 214 from Netzsch. Both use an inert atmosphere of nitrogen gas. Mercury, indium, tin, bismuth and zinc have been used to calibrate the DSC 214, whereas the TA Q100 has been calibrated by indium. The α - γ transition was studied using heating rates from 0.05 K min⁻¹ up to 200 K min⁻¹. The amount of material from 0.01 mg to 15 mg in the DSC capsule was varied to study the melting enthalpy of form γ as a function of the amount of material present in the DSC pan of which the volume is 45 μ L. It has been verified that decomposition was negligible during these DSC measurements (see Figure S4).

2.6 High-Pressure Differential Thermal Analysis (HP-DTA)

Transition temperatures as a function of pressure were measured by using a high-pressure differential thermal analyzer constructed in-house following the design by Würflinger (Würflinger, 1975). Therm 240 oil from Lauda was used as pressure-transmitting medium. PZA was mixed with Golden perfluorated liquid from Bioblock scientific to avoid the presence of air in the measurement pan, which may affect the thermodynamic equilibrium. DSC runs on the TA Q100 (see above) have been carried out to verify that the perfluorinated liquid is inert in the presence of PZA. The temperature range of the HP-DTA is 298 to 473 K, the pressure range is 0 to 250 MPa and the heating rate used in the measurement is 2 K min⁻¹.

2.7 Vapor pressure measurement

Vapor pressure measurements have been carried out isothermally in the temperature range 293.15 K - 383.15 K with a DVS Vacuum apparatus from Surface Measurements Systems, London, U.K., using a Knudsen cell whose orifice had a diameter of 440 micrometers and using benzoic acid vapor pressure as a standard.

2.8 Solubility measurement

The solubility in water of the α and γ forms of PZA has been measured in the range of 283.15 K to 313.15 K. A vial with water, which had been weighed, was placed in a jacketed crystallizer, while the temperature was controlled by a thermostat bath (CF41 Julabo). A predetermined mass of PZA weighed by a balance with a precision of 0.1 mg was added to the solution step by step. When the suspension remains visible in the solution for more than one hour, the solution was considered to be saturated. The final weight of PZA divided by the total amount of water is taken as the solubility at the set temperature.

3. Results

3.1 Calorimetric properties of the phase equilibria between α , γ , and the liquid

3.1.1 The melting equilibrium of form γ

A typical DSC curve of commercial PZA (form α) can be found in Figure 2. At a scanning rate of 10 K min^{-1} , α transforms into γ at around 425 K followed by the melting peak of γ at around 462 K (Figure 2). To determine the enthalpy and temperature of fusion of γ , measurements have been carried out at 10 K min^{-1} for a large number of samples of different mass. It became quickly clear that the enthalpy of fusion depends on the amount of material in the DSC capsule, similar to the cases of camphor (Rietveld et al., 2010) and adamantane (Espeau and Céolin, 2001). Therefore, the enthalpy of fusion was plotted as a function of the “specific volume” of the sample as shown in Figure 3 (the enthalpies and temperatures of fusion can be found in the supplementary materials Table S1). The “specific volume” of the sample in a DSC experiment ($V_{\text{pan}}/m_{\text{sample}}$) is the volume of a sealed DSC pan (V_{pan}), which includes its dead volume not taken up by solid PZA, divided by the mass of the weighed-in sample (m_{sample}). In most cases, when the vapor pressure of the solid is low, no consistent variation in the melting enthalpy will be observed; however, for pyrazinamide, a clear decrease of the measured specific enthalpy of fusion is observed with increasing “specific volume” (i.e. with decreasing mass, see Figure 3). The sublimation can in fact be observed by DSC, which is illustrated by two DSC curves of samples with a large difference in mass, as shown in Figure 2. The bottom curve exhibits a regular melting peak observed for a sample with a weight of 5.88 mg, whereas the top DSC curve represents a sample of 0.01 mg. In the inset, an upward shift from the baseline can be observed as a result of sublimation. Only a small peak-like drop to the baseline is observed at 449 K below the recorded melting temperature indicating that the sample has completely sublimated before it could have melted. Obviously, this rise of the baseline is also present in the curves with clear melting peaks, but in that case this baseline effect is dwarfed by the melting peak.

Taking the enthalpy data in Figure 3, one can establish a linear relationship with the specific volume in the DSC pan: $\Delta_{\gamma \rightarrow L}H (V_{\text{pan}}/m_{\text{sample}}) = -0.130(3) V_{\text{pan}}/m_{\text{sample}} + 236.1(9)$ leading to an enthalpy of fusion for a fully filled pan in the order of 236 J g^{-1} . However, it can be seen in the inset of Figure 3 that at the lowest specific volumes (i.e. fully filled DSC capsules), the enthalpy of fusion tends to even higher values in the order of 240 J g^{-1} . In fact, in the inset of Figure 3 at its lower range, one can observe a slight upward curvature in the line. For this reason, only the points up to a specific volume of $20 \text{ cm}^3 \text{ g}^{-1}$ have been used for the extrapolation, leading to the expression for the melting enthalpy, $\Delta_{\gamma \rightarrow L}H (\text{J g}^{-1})$, as a function of the “specific volume”, $V_{\text{pan}}/m_{\text{sample}} (\text{cm}^3 \text{ g}^{-1})$: $\Delta_{\gamma \rightarrow L}H (V_{\text{pan}}/m_{\text{sample}}) = -0.623(10) V_{\text{pan}}/m_{\text{sample}} + 241.0(1.0)$. Extrapolating this line to the specific volume of the γ form at its melting temperature (this translates to a capsule filled entirely with PZA without dead volume and is equal to $0.7003(31) \text{ cm}^3 \text{ g}^{-1}$ as reported below) leads to an enthalpy of fusion of $240.6(1.0) \text{ J g}^{-1}$.

Considering the scatter over the enthalpy of fusion of form γ , the enthalpies and temperatures of fusion of three single crystals have been determined too; in particular because the surface to bulk ratio is much smaller than in the case of powder, it may diminish the effect of sublimation. The data can be found in Table 3; there is still a considerable scatter over the melting enthalpy data and it is not clear whether the relation between the weighed-in mass and the enthalpy (Table 3) is accidental or not, but the average of $240(5) \text{ J g}^{-1}$ confirms the results obtained with capsules tightly filled with powder.

The overall behavior of the melting enthalpy increasing with an increasing amount of PZA is

clearly caused by the tendency of PZA to sublime as is shown in Figure 2. Less clear is the observation that at very high loads, the enthalpy appears to curve slightly upwards, confirmed by both completely filled capsules and single crystal data. How this curvature comes about with powder samples could be explained by a combination of sublimation and disorder reported for the γ form (Cherukuvada et al., 2010; Wahlberg et al., 2013).

The melting temperature, which does not vary with sample mass, is much easier to determine. The average over 27 points is equal to 462.0(5) K ($n = 27$). This value is in accordance with the literature data (see Table 1).

Table 3. The melting point and the enthalpy of fusion of single crystals of polymorphs α and γ measured by DSC^a

Sample	α			γ		
	T_{fus}/ K	$\Delta H/ \text{J g}^{-1}$	m / mg	T_{fus}/ K	$\Delta H/ \text{J g}^{-1}$	m / mg
1	457.05	250.6	0.98	462.35	244	2.69
2	456.65	255.7	0.66	462.55	239.9	2.12
3				462.65	235.9	1.69
Average	457(1)	253(4)		462.5(5)	240(5)	

^a heating rate is 100 K min⁻¹.

3.1.2 The melting transition of form α

The temperature and enthalpy of fusion of form α have been obtained using single crystals subjected to DSC runs at 100 K min⁻¹ (See Table 3). The high scanning rate was necessary to outrun the solid-solid transition from α to γ . The DSC has been specially calibrated for these measurements at 100 K min⁻¹ with the four calibrants listed for the DSC 214 from Netzsch (see experimental section). The melting point is found at 457(1) K and the enthalpy of fusion equals 253(4) J g⁻¹. It was not possible to investigate the influence of sublimation on the melting properties of α , due to the inaccuracy of the DSC at 100 K min⁻¹ and because changing to smaller crystals would cause them to turn into γ before melting. However, the high scanning speed and the fact that the sample was a single crystal, which decreases the surface to bulk ratio, may have limited the effect of sublimation considerably.

3.1.3 The α - γ equilibrium temperature

The transition temperature of α to γ had been previously shown to depend on the heating rate of the DSC (Castro et al., 2009). However, the value at infinitely low heating rate remains unknown. In the current study, once again different heating rates have been used to investigate the temperature of conversion of form α into γ and the results are presented in Figure 4 (the values can be found in the supplementary materials in Table S2). It is clear from Figure 4 that the transition temperature decreases with decreasing heating rate and there is no visible levelling off at very low heating rates even if the values observed are still lower than those reported by Castro et al. (Castro et al., 2009). DSC appears not to be the most appropriate method to determine the transition temperature between forms α and γ due to this particular kinetic behavior of the transition. Therefore, each polymorph has been kept in an oven in separate experiments at a decreasing series of temperatures starting roughly at the lowest transition temperature observed by DSC. The results are presented in Table 4. It

can be seen that at 392 K initial form α turns into form γ . Moreover, subjecting γ to a temperature of 391 K, a single crystal of form α is grown, while at 390 K, several α crystals can be observed. It can be concluded that the most likely equilibrium temperature between α and γ can be found between 391 and 392 K. Lacking any further precision, the average between these values will be rounded off to the nearest digit: $T_{\alpha \rightarrow \gamma} = 392(1)$ K.

Table 4. The stability of the polymorphs α and γ at constant temperature

T/ K	Initial polymorph	Final polymorph	Comments
403	α	γ	
398	α	γ	
394	α	γ	
392	α	$\gamma + \alpha$	γ is single crystal
391	γ	$\gamma + \alpha$	One single crystal of α
390	γ	$\gamma + \alpha$	Few crystals of α
373	γ	α	
353	γ	α	

The enthalpy change associated to the α - γ transition has been determined at a scanning rate of 10 K min^{-1} . It did not depend on the sample mass as in the case of the melting point of γ , most likely because the lower temperature did not cause as much sublimation. Interestingly, the enthalpy difference between the two polymorphs remained constant even if the transition temperature ranged from 405 to 440 K (the data can be found in the supplementary materials, Table S2 and Figure S1). The average of the α - γ transition enthalpy has been found to be $\Delta_{\alpha \rightarrow \gamma}H = 13.2(6) \text{ J g}^{-1}$ ($n = 83$).

The constant transition enthalpy between α and γ indicates that their difference in heat capacity does not change with the temperature. It also implies that the sum of the enthalpies of the cycle α to γ to liquid to α must be more or less equal to zero: $\Delta_{\alpha \rightarrow \gamma}H + \Delta_{\gamma \rightarrow L}H - \Delta_{\alpha \rightarrow L}H = 13.2 + 240 - 253 = 0.2 \cong 0$. The fact that this sum indeed equals zero indicates that the enthalpy differences between phases α , γ , and the liquid appear to be consistent. One may therefore conclude that most likely the enthalpy difference between α and γ is temperature independent between their equilibrium temperature and the melting point of PZA. The value is equal to the values reported in literature (Castro et al., 2009; Lourenço et al., 2012). However, the transition temperature between the two solids at 392 K appears to be at least 20 degrees lower, than previously reported in the literature (Table 1) (Castro et al., 2009).

3.1.4 The glass transition of pyrazinamide

In principle, the glassy state of a chemical compound can be obtained by quenching its melt. However, PZA is not a good glass former and it recrystallizes rapidly even if quenched in liquid nitrogen after melting. Therefore, it has been difficult to obtain conclusive results on the temperature of the glass transition. However, in most measurements, a departure from the baseline, indicating the occurrence of a phase transition and thus the presence of molecular mobility, could be observed between 250 and 260 K in accordance with the paper

of Borba et al, who observed the formation of δ from glassy film at 260 K (Borba et al., 2009). It seems therefore appropriate to set the glass transition temperature at 260 K as the highest possible estimate.

3.1.5 The α - γ transition and the fusion of γ under pressure

High-pressure differential thermal analysis curves containing the peaks for the α to γ transition and the fusion of γ are shown in Figure 5a. The observed transitions have been plotted as a function of the pressure and the temperature and are presented in Figure 5b. The values can be found in the supplementary materials (fusion of γ : Table S3 and the α - γ transition: Table S4). The solid-solid transition was difficult to measure and only a few points could be obtained. In both cases the data has been fitted to a straight line in the form of the pressure P/MPa as a function of the temperature T/K :

$$\gamma \rightarrow \text{L}: P = 3.5(3) T - 1623(100) \quad (2)$$

$$\alpha \rightarrow \gamma: P = -3.6(7) T + 1510(283) \quad (3)$$

3.2 The specific volumes of polymorphs α and γ

3.2.1 Temperature dependence of the specific volume

The specific volumes of forms α and γ as a function of the temperature have been obtained by high-resolution PXRD. The X-ray diffraction patterns are provided in Figure 6 and the resulting specific volumes are presented in Figure 7 (the values can be found in the supplementary materials Table S5). The data has been fitted to the following expressions of specific volume V_i ($\text{cm}^3 \text{g}^{-1}$) as a function of the temperature T (K):

$$V_\alpha = 0.6624(7) + 6.8(6) \times 10^{-5} T + 8.44 (1.06) \times 10^{-8} T^2 \quad (4)$$

$$V_\gamma = 0.6520(7) + 4.8(5) \times 10^{-5} T + 1.22(9) \times 10^{-7} T^2 \quad (5)$$

Comparing the specific volume of form α and γ measured in this work and the literature (see Figure 7), the specific volume of form α is larger than that of form γ : $V_\alpha > V_\gamma$. In other words, the density of α is smaller than that of form γ : $d_\alpha < d_\gamma$. Interestingly, the difference in specific volume hardly changes from 100 K up to 400 K: $\Delta_{\alpha \rightarrow \gamma} V(T) = -0.01242(23) - 1.1(9) \times 10^{-6} T$ and the average difference in volume between α and γ is $\Delta_{\alpha \rightarrow \gamma} V = -0.0127(4) \text{ cm}^3 \text{g}^{-1}$ with an error of less than 2.5 % (see also Figure 7). Although the literature data appears to be somewhat scattered in Figure 7, the γ form is clearly the denser one.

3.2.2 Pressure dependence of the specific volume

The powder diffraction patterns obtained under different pressures at 295 K can be found in the supplementary materials (Figure S2 and S3) and the values of the specific volumes as a function of pressure obtained from the patterns have been reported in Table S6 and are also depicted in Figure 8. The specific volumes V_i ($\text{cm}^3 \text{g}^{-1}$) of forms α and γ have been expressed as a function of the pressure P/MPa in the following two equations:

$$V_{\alpha} = 0.6883(2) - 5.27(4) \times 10^{-5} P + 9.0(2) \times 10^{-9} P^2 \quad (6)$$

$$V_{\gamma} = 0.6826(6) - 5.17(12) \times 10^{-5} P + 8.5(6) \times 10^{-9} P^2 \quad (7)$$

The specific volumes of the two forms decrease with increasing pressure while form γ is denser than form α as expected from the results shown just above. It can be seen that eqs. 6 and 7 are very similar. Using a 3rd order Birch-Murnaghan equation of state (see the Supplementary Materials for the equation) (Angel et al., 2014a; Angel et al., 2014b; Birch, 1947) a measure for the compressibility can be obtained, which leads for α to a specific volume at 0 MPa and 295 K $V_{0,295\text{ K}} = 0.6891(2) \text{ cm}^3 \text{ g}^{-1}$, a bulk modulus (i.e. inverse compressibility) $K_{0,295\text{ K}} = 11.1(2) \times 10^3 \text{ MPa}$ and its derivative with pressure of $K'_{0,295\text{ K}} = 9.8(3)$. For γ , the results are: $V_{0,295\text{ K}} = 0.6869(2) \text{ cm}^3 \text{ g}^{-1}$, $K_{0,295\text{ K}} = 9.30(4) \times 10^3 \text{ MPa}$ and $K'_{0,295\text{ K}} = 12.1(1)$. The bulk moduli and derivatives of the two polymorphs are similar.

3.3 The vapor pressure of the α and γ polymorphs

A few papers contain data on the vapor pressure of the α form (Blokhina et al., 2015a; Negoro, 1959; Negoro, 1960), however, data obtained by different methods are difficult to compare. Thus, the vapor pressure of α and γ as a function of the temperature is measured in this work with the same equipment and the result is shown in Table S7. Using the Clausius–Clapeyron equation ($\ln P = -\Delta_{S \rightarrow V}H/RT + B$, $\Delta_{S \rightarrow V}H$ is the enthalpy of sublimation, B is a constant), the vapor pressure $P(\text{Pa})$ can be expressed as a function of the temperature $T(\text{K})$:

$$\alpha \rightarrow V: \ln P = -94945(1024) / RT + 32.3(4) \quad (R^2 = 0.9991) \quad (8)$$

$$\gamma \rightarrow V: \ln P = -92192(2024) / RT + 31.5(7) \quad (R^2 = 0.9986) \quad (9)$$

with the numerator the enthalpy of sublimation in J mol^{-1} and R the gas constant, $8.3145 \text{ J K}^{-1} \text{ mol}^{-1}$. The sublimation enthalpies from eqs. 8 and 9 reflect the differences in enthalpy between the respective polymorph and the vapor phase. It implies that the difference between these two enthalpies must be similar to the transition enthalpy between the two solid phases: $\Delta_{\alpha \rightarrow \gamma}H = \Delta_{\alpha \rightarrow V}H - \Delta_{\gamma \rightarrow V}H = 94945 - 92192 = 2.75(2.27) \text{ kJ mol}^{-1}$ or $22(19) \text{ J g}^{-1}$. Obviously, the error over the large enthalpy values is considerable, which is reflected in the large error over the transition enthalpy of 19 J g^{-1} ; however, the value is equal within error with that of the DSC even if the vapor pressure is simply not precise enough to determine an accurate enthalpy difference. In comparison with the literature values (Table 1), the enthalpies of vaporization found here, 771 J g^{-1} for α and 749 J g^{-1} for γ , are similar; however, the spread in the values in Table 1 is large and it seems essential that data for different polymorphs are obtained with a single apparatus for reliable comparison.

The intersection between the two lines eqs. 8 and 9, where the vapor pressure of the two polymorphs is equal, should coincide with the equilibrium temperature for α and γ . It is found at about 398 K, which is somewhat higher than 392 K, the result obtained in Table 4.

3.4 The solubility of α and γ

The solubilities in water of the α and γ polymorphs measured at different temperatures and those found in the literature (Hermanto et al., 2015; Zhang et al., 2017) are provided in Table S8 and Figure 9. The solubility of γ is higher than the solubility of α . The solubility of α measured in this work is similar to the data measured in the literature, but the solubility of γ is different. This may be explained by the metastability of γ , which may cause a larger error over the result due to stability issues. The solubility data can be fitted using the van't Hoff equation:

$$\ln x_i = -\frac{\Delta_{d(i)}H}{RT} + \frac{\Delta_{d(i)}S}{R} \quad (10)$$

where x_i is the mole fraction solubility of form i (/mmol mol⁻¹), $\Delta_{d(i)}H$ and $\Delta_{d(i)}S$ represent the dissolution enthalpy and entropy of form i in water, respectively. T is the temperature (/K), and R is the gas constant.

$$\alpha: \ln x = -28917(643) / RT + 12.5(3) \quad (R^2 = 0.9985) \quad (11)$$

$$\gamma: \ln x = -26714(1034) / RT + 11.7(5) \quad (R^2 = 0.9955) \quad (12)$$

Like the enthalpy of sublimation, the transition enthalpy can be calculated: $\Delta_{\alpha \rightarrow \gamma}H = \Delta_{d(\alpha)}H - \Delta_{d(\gamma)}H = 28.917 - 26.714 = 2.21(1.3)$ kJ mol⁻¹ or 18 (10) J g⁻¹. Errors are again large due to the comparison between two large values; however, the overall difference in enthalpy between the two polymorphs is close to the value of 13.2 J g⁻¹ obtained by DSC. The equilibrium transition temperature between α and γ in the presence of water can be calculated using eq. 11 and 12, the intersection of these two lines being the transition temperature. It is found at 330(4) K. This temperature is lower than that obtained through the oven and the vapor pressure experiments. This could be due to the difficulties in interpreting the solubility data due to metastability and the interaction between solvent and solute, which may affect the chemical potentials of the polymorphs as described by the Gibbs-Duhem equation.

4. Discussion

4.1 Interpretation of the phase behavior of polymorphs α , γ , and the liquid

Using the data presented above, a pressure-temperature phase diagram can be constructed describing the behavior of the three condensed phases that have been investigated. Eq. 2 describes the pressure-temperature behavior of the melting equilibrium of γ . Considering that this transition is observed in the direction of a solid-liquid transformation and thus no significant kinetic barrier exists for the transition, there is little doubt that the obtained equation reflects the equilibrium behavior within error.

The same cannot be said about the α - γ transition, as is very clear from Figure 4, where the transition temperature decreases as the heating rate decreases. This implies that eq. 3, $P(T)_{\alpha \rightarrow \gamma}$, should be shifted to lower temperatures assuming that the slope will stay the same. In fact, the slope of the α - γ equilibrium can be verified with the Clapeyron equation (eq. 1), using the calorimetric and volumetric data discussed above: $T_{\alpha \rightarrow \gamma} = 392(1)$ K, $\Delta_{\alpha \rightarrow \gamma}H = 13.2(6)$

J g^{-1} , and with eqs. 4 and 5 $\Delta_{\alpha \rightarrow \gamma} v (392 \text{ K}) = -0.0124 (38) \text{ cm}^3 \text{g}^{-1}$, as $v_{\alpha} (392 \text{ K}) = 0.7021(29) \text{ cm}^3 \text{g}^{-1}$ and $v_{\gamma} (392 \text{ K}) = 0.6897(25) \text{ cm}^3 \text{g}^{-1}$. This leads to a slope of $-2.7(9) \text{ MPa K}^{-1}$. Even if the values of the slopes ($-3.6(7) \text{ MPa K}^{-1}$ in eq. 3) overlap within error, it is most likely that the slope of the α - γ equilibrium is closer to -2.7 MPa K^{-1} , because the transition points obtained by HP-DTA may suffer an overestimation in temperature as observed in the regular DSC measurements for this solid-solid transition. Thus, the pressure (P/ MPa) of the α - γ equilibrium can be expressed as a function of the temperature (T/ K) in the following adjusted way:

$$\alpha \rightarrow \gamma: P = -2.7(9) T + 1064(327) \quad (13)$$

In which the line is shifted to pass through 392 K at 0 MPa (representing the vapor pressure of PZA).

Taking the intersection of eqs. 2 and 13, one finds the triple point where the phases α , γ , and the liquid are in equilibrium, leading to 431 K and -105 MPa . Using this triple point in turn with the melting temperature of form α , 457 K at 0 MPa, the pressure (P/ MPa) for the melting equilibrium of form α as a function of temperature (T/ K) can be obtained:

$$\alpha \rightarrow \text{L}: P = 4.0 T - 1823 \quad (14)$$

It can be seen that this melting equilibrium is the steepest in the phase diagram as expected for the three diverging equilibria, α - γ , α -L, and γ -L, with increasing pressure.

4.2 The volume difference between solid and liquid on melting

For statistical reasons, it is of interest to study the change in the specific volume of the melting solid. In particular for cases for which it is not possible to have experimental access to the slope of the melting equilibrium using statistical data, an estimate of the slope can be obtained and a topological phase diagram can be constructed through thermodynamic reasoning.

In the case of pyrazinamide, the slope of the melting of the γ phase has been found to be $3.5 (3) \text{ MPa K}^{-1}$ (eq. 2) based on the HP-DTA data. Taking the melting enthalpy of $240(5) \text{ J g}^{-1}$ obtained above, the melting temperature of $462.0(5) \text{ K}$ and the specific volume of the γ form at the melting temperature (eq. 5), $V_{\gamma} (462.0 \text{ K}) = 0.7003(31) \text{ cm}^3 \text{g}^{-1}$, one obtains through the Clapeyron equation the volume change on melting, $\Delta_{\gamma \rightarrow \text{L}} V = 0.1473(92) \text{ cm}^3 \text{g}^{-1}$, and the specific volume of the liquid at the melting point: $V_{\text{L}} (462.0 \text{ K}) = 0.8476(97) \text{ cm}^3 \text{g}^{-1}$.

For the melting of the α form, information on the thermal expansion of the liquid can be used. From the results in this paper and from those of Borba, it can be concluded that the glass transition temperature can be found around 260 K (Borba et al., 2010). Because at the glass transition, the liquid turns into a glass, by approximation its density can be set equal to that of the least dense polymorph of pyrazinamide, which is form α (see Figure 7). At 260 K, form α will have a specific volume of $V_{\alpha} (260 \text{ K}) = 0.6858 \text{ cm}^3 \text{g}^{-1}$ (eq. 4). With the specific volume of the liquid at the melting point of the γ form, the specific volume of the liquid ($V_{\text{L}}/ \text{cm}^3 \text{g}^{-1}$) as a function of the temperature (T/ K) can be described by a straight line (seen Figure 10):

$$V_L = 0.47756 + 8.0101 \times 10^{-4}T \quad (15)$$

Using the known data on the melting of the α form, $T_{\alpha \rightarrow L} = 457(1)$ K, $\Delta_{\alpha \rightarrow L}H = 253(4)$ J g⁻¹, $V_{\alpha}(T_{\alpha \rightarrow L}) = 0.7112(35)$ cm³ g⁻¹ and $V_L(T_{\alpha \rightarrow L}) = 0.8435(3)$ cm³ g⁻¹ a change in the volume on the melting of α can be determined $\Delta_{\alpha \rightarrow L}V = 0.1323(36)$ cm³ g⁻¹. This leads to a slope for the melting equilibrium of 4.2(2) MPa K⁻¹. Comparing this to the slope in eq. 14 of 4.0 MPa K⁻¹, which has been obtained by extrapolation of the γ -L equilibrium and the α - γ equilibrium, demonstrates the strength of the topological method and the redundancy in the data due to the thermodynamic requirements they need to fulfill.

The ratio of the volume of the liquid by that of the solid form which melts is $V_L/V_{\gamma} = 1.21$ for γ and $V_L/V_{\alpha} = 1.19$ for α . These values are large in comparison with most small organic molecules and only form III of piracetam with a ratio of 1.18 comes anywhere near these values (Toscani et al., 2016). Goodman et al. (Goodman et al., 2004) found an average expansion on melting of about 12% for small organic molecules based on 21 compounds. Based on different distributions of small pharmaceutical molecules, similar expansions with an average in the order of 11% have been recorded (Céolin and Rietveld, 2015; Gavezzotti, 2007). The reason for the large difference in the specific volume between the solid state and the liquid state must lie in the flatness of the molecule, which makes efficient stacking possible in the solid, but which is obviously lost in the liquid state. The density of the γ form is indeed rather high for an organic substance with 1.43 g cm⁻³ at its melting point and 1.48 g cm⁻³ at room temperature.

4.3 The pressure-temperature phase diagram

The resulting topological pressure-temperature phase diagram of α - γ -L-V is presented in Figure 11. This phase diagram is built based on eqs. 2, 13, and 14 for the condensed phases and eqs. 8 and 9 for the vapor phases. The final liquid – vapor (L-V) equilibrium curve can be calculated as follows. The enthalpy of vaporization is $\Delta_{L \rightarrow V}H = \Delta_{\gamma \rightarrow V}H - \Delta_{\gamma \rightarrow L}H$; $\Delta_{\gamma \rightarrow V}H$ can be obtained from eq. 12 and amounts to 749(17) J g⁻¹ and $\Delta_{\gamma \rightarrow L}H$ is 240(5) J g⁻¹, so that $\Delta_{L \rightarrow V}H$ is 509(17) J g⁻¹. Eqs. 2 and 9 can be used to calculate the triple point of γ -L-V through which the L-V equilibrium curve must pass leading to the expression:

$$L \rightarrow V: \ln P = -7535 / T + 23.8 \quad (16)$$

with P in Pa and T in K.

5. Conclusions

This paper gives a clear demonstration of the fact that it can be very hard to obtain equilibrium data for molecular systems. The API Pyrazinamide suffers multiple problems: disorder in the high-temperature form, a high sublimation pressure at high temperatures, and extremely slow solid-solid phase transformations between almost all solid forms.

The high vapor pressure of pyrazinamide at elevated temperatures affects the melting enthalpy as demonstrated in Figure 3. In principle such behavior can be compensated by measurements that take the volume available to the sample into account as has been done

in this paper. Only single crystals and fully packed DSC capsules appear to approach the ideal melting enthalpy.

Extremely slow solid-solid transitions are nothing new for researchers working with differential calorimetry, however, finding the proper transition temperature with a transition that is found at ever lower temperatures when decreasing the scanning rate of the DSC is not an easy endeavor (Barrio et al., 2012; Rietveld et al., 2011). In the present case, only measurements outside of the DSC, e.g. heating samples in an oven for weeks appears to have provided a clue on where to find the solid-solid equilibrium between α and γ forms. Whether this approach will deliver any equilibrium temperatures in relation to the other solid forms is absolutely not clear yet. The data on vapor pressure and solubility confirm the equilibrium temperature; however, extrapolation and the errors over the vapor pressure and solubility data give rise to a rather large error margin.

The pressure-temperature phase diagram presented in Figure 11 only contains the two most studied phases of pyrazinamide, because equilibrium data on the other two forms β and δ still remain elusive due to the slow phase transition rates. In previous papers on the subject, no convincing evidence has been provided that equilibrium data on these two forms has been reported, leaving any conclusions on the stability of these two forms pending. Nonetheless, the present phase diagram involving the equilibria between α , γ , and the liquid remains valid, within the limits of the precision of the data, regardless of the stability hierarchy in relation to the other two solid phases. It is therefore clear, that from the point of view of form α , form γ is a high-pressure, high-temperature form, which under ambient temperature becomes stable at a pressure in the order of 260 MPa. This value is not high from a processing point of view, in particular if one considers that the equilibrium pressure will decrease with increasing temperature. Nonetheless, no α - γ transition has been observed under pressures up to 2 GPa in line with the observation that transition rates are very slow.

Declaration of Interests

The authors declare no competing financial interests

Acknowledgements

K. Li thanks the ERASMUS organization for a travel grant for three months of research in Barcelona. The authors thank Jean-Paul Itié for his support on beamline Psiché, synchrotron Soleil (Gif sur Yvette).

Funding: This work was supported by the Region Normandie, synchrotron Soleil (beamline Psiché), MINECO Project No. FIS2017-82625-P, and AGAUR DGU Project No. 2017SGR-42

References

- A.Nangia, A.Srinivasulu, 2005. CSD Communication(Private Communication)
- Abourahma, H., Shah, D.D., Melendez, J., Johnson, E.J., Holman, K.T., 2015. A Tale of Two Stoichiometrically Diverse Cocrystals. *Crystal Growth & Design* 15, 3101-3104.

Adalder, T.K., Sankolli, R., Dastidar, P., 2012. Homo-or heterosynthon? A crystallographic study on a series of new cocrystals derived from pyrazinecarboxamide and various carboxylic acids equipped with additional hydrogen bonding sites. *Crystal Growth & Design* 12, 2533-2542.

Angel, R.J., Gonzalez-Platas, J., Alvaro, M., 2014a. EosFit7c and a Fortran module (library) for equation of state calculations. *Z Krist-Cryst Mater* 229, 405-419.

Angel, R.J., Mazzucchelli, M.L., Alvaro, M., Nimis, P., Nestola, F., 2014b. Geobarometry from host-inclusion systems: The role of elastic relaxation. *Am. Mineral.* 99, 2146-2149.

Baaklini, G., 2015. Les Effets du Spray Drying sur le polymorphisme des composés pharmaceutiques et organiques. Rouen.

Baaklini, G., Dupray, V., Coquerel, G., 2015. Inhibition of the spontaneous polymorphic transition of pyrazinamide γ form at room temperature by co-spray drying with 1, 3-dimethylurea. *International journal of pharmaceutics* 479, 163-170.

Barrio, M., Maccaroni, E., Rietveld, I.B., Malpezzi, L., Masciocchi, N., Céolin, R., Tamarit, J.I., 2012. Pressure-temperature state diagram for the phase relationships between benfluorex hydrochloride forms I and II: a case of enantiotropic behavior. *Journal of pharmaceutical sciences* 101, 1073-1078.

Barrio, M., Tamarit, J.L., Ceolin, R., Robert, B., Guéchet, C., Teulon, J.M., Rietveld, I.B., 2017. Experimental and topological determination of the pressure-temperature phase diagram of morniflumate, a pharmaceutical ingredient with anti-inflammatory properties. *Journal of Chemical Thermodynamics* 112, S0021961417301544.

Battilocchio, C., Hawkins, J.M., Ley, S.V., 2014. Mild and selective heterogeneous catalytic hydration of nitriles to amides by flowing through manganese dioxide. *Organic letters* 16, 1060-1063.

Birch, F., 1947. Finite Elastic Strain of Cubic Crystals. *Phys. Rev.* 71, 809-824.

Blokhina, S., Sharapova, A., Ol'khovich, M., Volkova, T., Perlovich, G., 2015a. Vapor pressures and thermodynamic sublimation of antitubercular drugs. *J. Therm. Anal. Calorim.* 120, 1053-1060.

Blokhina, S.V., Ol'khovich, M.V., Sharapova, A.V., Volkova, T.V., Perlovich, G.L., 2015b. Solution thermodynamics of pyrazinamide, isoniazid, and p-aminobenzoic acid in buffers and octanol. *The Journal of Chemical Thermodynamics* 91, 396-403.

Borba, A., Albrecht, M., Gomez-Zavaglia, A., Suhm, M.A., Fausto, R., 2010. Low Temperature Infrared Spectroscopy Study of Pyrazinamide: From the Isolated Monomer to the Stable Low Temperature Crystalline Phase. *J. Phys. Chem. A* 114, 151-161.

Borba, A., Albrecht, M., Gómez-Zavaglia, A., Suhm, M.A., Fausto, R., 2009. Low temperature infrared spectroscopy study of pyrazinamide: from the isolated monomer to the stable low temperature crystalline phase. *The Journal of Physical Chemistry A* 114, 151-161.

Brits, M., Liebenberg, W., De Villiers, M.M., 2010. Characterization of polymorph transformations that decrease the stability of tablets containing the WHO essential drug mebendazole. *Journal of pharmaceutical sciences* 99, 1138-1151.

Castro, R.A., Maria, T.M., Évora, A.O., Feiteira, J.C., Silva, M.R., Beja, A.M., Canotilho, J., Eusébio, M.E.S., 2009. A new insight into pyrazinamide polymorphic forms and their thermodynamic relationships. *Crystal Growth & Design* 10, 274-282.

Censi, R., Di Martino, P., 2015. Polymorph impact on the bioavailability and stability of poorly soluble drugs. *Molecules* 20, 18759-18776.

Céolin, R., Rietveld, I.B., 2015. The topological pressure-temperature phase diagram of ritonavir, an extraordinary case of crystalline dimorphism. *Annales Pharmaceutiques Françaises* 73, 22-30.

Cherukuvada, S., Nangia, A., 2012. Fast dissolving eutectic compositions of two anti-tubercular drugs. *CrystEngComm* 14, 2579-2588.

Cherukuvada, S., Thakuria, R., Nangia, A., 2010. Pyrazinamide polymorphs: relative stability and vibrational spectroscopy. *Crystal Growth & Design* 10, 3931-3941.

Choquesillo-Lazarte, D., Nemec, V., Cinčić, D., 2017. Halogen bonded cocrystals of active pharmaceutical ingredients: pyrazinamide, lidocaine and pentoxifylline in combination with haloperfluorinated compounds. *CrystEngComm* 19, 5293-5299.

Datta, S., Grant, D.J., 2004. Crystal structures of drugs: advances in determination, prediction and engineering. *Nature Reviews Drug Discovery* 3, 42.

E. Castro, R.A., Ribeiro, J.D., Maria, T.M., Ramos Silva, M., Yuste-Vivas, C., Canotilho, J., Eusébio, M.E.S., 2011. Naproxen cocrystals with pyridinecarboxamide isomers. *Crystal Growth & Design* 11, 5396-5404.

Eddleston, M.D., Arhangel'skis, M., Fabian, L., Tizzard, G.J., Coles, S.J., Jones, W., 2015. Investigation of an amide-pseudo amide hydrogen bonding motif within a series of theophylline: amide cocrystals. *Crystal Growth & Design* 16, 51-58.

Espeau, P., Céolin, R., 2001. Thermodynamic studies of solids with non-negligible vapour pressure: T–v and p–T diagrams of the dimorphism of adamantane. *Thermochimica acta* 376, 147-154.

Évora, A.O., Castro, R.A., Maria, T.M., Rosado, M.T., Ramos Silva, M., Matos Beja, A., Canotilho, J., Eusébio, M.E.S., 2011. Pyrazinamide-diflunisal: a new dual-drug co-crystal. *Crystal Growth & Design* 11, 4780-4788.

Gavezzotti, A., 2007. Molecular aggregation: structure analysis and molecular simulation of crystals and liquids. , OUP Oxford.

Goodman, B.T., Wilding, W.V., Oscarson, J.L., Rowley, R.L., Goodman, B.T., Wilding, W.V., Oscarson, J.L., Rowley, R.L., 2004. A Note on the Relationship between Organic Solid Density and Liquid Density at the Triple Point. *Journal of Chemical & Engineering Data* 49, págs. 1512-1514.

Hermanto, M.W., Yeoh, A., Soh, B., Chow, P.S., Tan, R.B., 2015. Robust Crystallization Process Development for the Metastable δ -form of Pyrazinamide. *Organic Process Research & Development* 19, 1987-1996.

Hilfiker, R., 2006. Polymorphism in the pharmaceutical industry. Wiley Online Library.

Inès, G., Maria, B., Bernard, D., Josep-Lluís, T., René, C., Rietveld, I.B., 2013. Benzocaine polymorphism: pressure-temperature phase diagram involving forms II and III. *Int J Pharm* 456, 480-488.

Jarzembska, K.N., Hoser, A.A., Kamiński, R., Madsen, A.Ø., Durka, K., Woźniak, K., 2014. Combined experimental and computational studies of pyrazinamide and nicotinamide in the context of crystal engineering and thermodynamics. *Crystal Growth & Design* 14, 3453-3465.

Kulla, H., Greiser, S., Benemann, S., Rademann, K., Emmerling, F., 2016. In situ investigation of a self-accelerated cocrystal formation by grinding pyrazinamide with oxalic acid. *Molecules* 21, 917.

Kulla, H., Greiser, S., Benemann, S., Rademann, K., Emmerling, F., 2017. Knowing When To Stop · Trapping Metastable Polymorphs in Mechanochemical Reactions. *Crystal Growth & Design* 17, 1190-1196.

Lavor, E.P., Freire, F.D., Aragão, C.F.S., Raffin, F.N., 2012. Application of thermal analysis to the study of anti-tuberculosis drug compatibility. Part 1. *Journal of thermal analysis and calorimetry* 108, 207-212.

Liu, F., Song, Y., Liu, Y.-N., Li, Y.-T., Wu, Z.-Y., Yan, C.-W., 2018. Drug-bridge-drug ternary cocrystallization strategy for antituberculosis drugs combination. *Crystal Growth & Design* 18, 1283-1286.

Lourenço, C., Melo, C.I., Bogel-Łukasik, R., Bogel-Łukasik, E., 2012. Solubility Advantage of Pyrazine-2-carboxamide: Application of Alternative Solvents on the Way to the Future Pharmaceutical Development. *Journal of Chemical & Engineering Data* 57, 1525-1533.

Lourenço, C., Melo, C.I., Bogel-Łukasik, R., Bogel-Łukasik, E., 2012. Solubility advantage of pyrazine-2-carboxamide: application of alternative solvents on the way to the future pharmaceutical development. *Journal of Chemical & Engineering Data* 57, 1525-1533.

Luo, Y.-H., Liu, Q.-L., Yang, L.-J., Wang, W., Ling, Y., Sun, B.-W., 2015. Quantitative comparisons between α , β , γ , and δ pyrazinamide (PZA) polymorphs. *Research on Chemical Intermediates* 41, 7059-7072.

Luo, Y.-H., Sun, B.-W., 2013. Pharmaceutical Co-Crystals of Pyrazinecarboxamide (PZA) with Various Carboxylic Acids: Crystallography, Hirshfeld Surfaces, and Dissolution Study. *Cryst. Growth Des.* 13, 2098-2106.

Morris, K.R., Griesser, U.J., Eckhardt, C.J., Stowell, J.G., 2001. Theoretical approaches to physical transformations of active pharmaceutical ingredients during manufacturing processes. *Advanced drug delivery reviews* 48, 91-114.

Nakata, K., Takaki, Y., 1987. *Mem.Osaka Kyoiku Univ.Ser.* 3, 93.

Negoro, H., 1959. Solubility phenomena of pyridine-and pyrazinemonocarboxamides. I. Heat of sublimation of picolinamide, nicotinamide, isonicotinamide, and pyrazinecarboxamide. *Takamine Kenkyusho Nempo* 11, 66-75.

Negoro, H., Miki, T., Ueda, S., 1960. Solubility phenomena of pyridine- and pyrazinemonocarboxamides. I. Heat of sublimation of picolinamide, nicotinamide, isonicotinamide, and pyrazinecarboxamide. *Yakugaku Zasshi* 80, , 665-669.

Pajula, K., Taskinen, M., Lehto, V.-P., Ketolainen, J., Korhonen, O., 2010. Predicting the formation and stability of amorphous small molecule binary mixtures from computationally determined Flory–Huggins interaction parameter and phase diagram. *Molecular pharmaceutics* 7, 795-804.

Rajalakshmi, G., Hathwar, V.R., Kumaradhas, P., 2014. Intermolecular interactions, charge - density distribution and the electrostatic properties of pyrazinamide anti - TB drug molecule: an experimental and theoretical charge - density study. *Acta Crystallographica Section B* 70, 568-579.

Rajbongshi, T., Sarmah, K.K., Sarkar, A., Ganduri, R., Cherukuvada, S., Thakur, T.S., Thakuria, R., 2018. Preparation of Pyrazinamide Eutectics versus Cocrystals Based on Supramolecular Synthons Variations. *Crystal Growth & Design* 18, 6640-6651.

Ribeiro da Silva, M.D., Miranda, M.S., Vaz, C.M., Matos, M.A.R., Acree Jr, W., 2005. Experimental thermochemical study of three monosubstituted pyrazines. *The Journal of Chemical Thermodynamics* 37, 49-53.

Rietveld, I.B., Barrio, M., Tamarit, J.L., Nicolai, B., Van de Streek, J., Mahé, N., Ceolin, R., Do, B., 2011. Dimorphism of the prodrug I - tyrosine ethyl ester: Pressure–temperature state diagram and crystal structure of phase II. *Journal of pharmaceutical sciences* 100, 4774-4782.

Rietveld, I.B., Barrio, M., Veglio, N., Espeau, P., Tamarit, J.L., Céolin, R., 2010. Temperature and composition-dependent properties of the two-component system D- and L-camphor at 'ordinary' pressure. *Thermochimica Acta* 511, 43-50.

Rø, G., Sørum, H., 1972a. The crystal and molecular structure of β - pyrazinecarboxamide. *Acta Crystallographica Section B* 28, 991-998.

Rø, G., Sørum, H., 1972b. The crystal and molecular structure of δ - pyrazinecarboxamide. *Acta Crystallographica Section B* 28, 1677-1684.

Rodriguez-Carvajal, J., Roisnel, T., Gonzales-Platas, J., 2005. FullProf suite (2005 version). CEA-CNRS, CEN Saclay, France: Laboratoire Léon Brillouin.

Sharma, P., Nandi, R., Gangopadhyay, D., Singh, A., Singh, R.K., 2018. Temperature dependent polymorphism of pyrazinamide: An in situ Raman and DFT study. *Spectrochimica Acta Part A: Molecular and Biomolecular Spectroscopy* 190, 177-180.

Smets, M., Baaklini, G., Tijink, A., Sweers, L., Vossen, C., Brandel, C., Meekes, H., Cuppen, H., Coquerel, G., 2018. Inhibition of the Vapor-Mediated Phase Transition of the High Temperature Form of Pyrazinamide. *Crystal growth & design* 18, 1109-1116.

Su, Y., Xu, J., Shi, Q., Yu, L., Cai, T., 2018. Polymorphism of griseofulvin: concomitant crystallization from the melt and a single crystal structure of a metastable polymorph with anomalously large thermal expansion. *Chemical Communications* 54, 358-361.

Takaki, Y., Sasada, Y., Watanabé, T., 1960. The crystal structure of α -pyrazinamide. *Acta Crystallographica* 13, 693-702.

Tamura, C., Kuwano, H., Sasada, Y., 1961. Crystallographic data of carboxylic acids and carboxyamides of picoline and pyrazine derivatives. *Acta Crystallographica* 14, 693-693.

Tan, X., Wang, K., Li, S., Yuan, H., Yan, T., Liu, J., Yang, K., Liu, B., Zou, G., Zou, B., 2012. Exploration of the pyrazinamide polymorphism at high pressure. *The Journal of Physical Chemistry B* 116, 14441-14450.

Thakuria, R., Cherukuvada, S., Nangia, A., 2012. Crystal Structures of Pyrogallol, Its Hydrate, and Stable Multiple Z' Cocrystals with N-Heterocycles Containing Metastable Conformers of Pyrogallol. *Crystal Growth & Design* 12, 3944-3953.

Tiwari, R.K., Deo, N., Singh, T.P., 1980. *J. Sci. Res. Bhopal, India* 2, 161.

Tiwari, R.K., Patel, T.C., Singh, T.P., 1982. *Indian J. Phys. Sect. A* 56, 413.

Toscani, S., Céolin, R., Ter Minassian, L., Barrio, M., Veglio, N., Tamarit, J.-L., Louër, D., Rietveld, I.B., 2016. Stability hierarchy between Piracetam forms I, II, and III from experimental pressure–temperature diagrams and topological inferences. *International journal of pharmaceutics* 497, 96-105.

Wahlberg, N., Ciochoń, P., Petriček, V., Madsen, A.Ø., 2013. Polymorph stability prediction: on the importance of accurate structures: a case study of pyrazinamide. *Crystal Growth & Design* 14, 381-388.

Wang, J.-R., Ye, C., Mei, X., 2014. Structural and physicochemical aspects of hydrochlorothiazide co-crystals. *CrystEngComm* 16, 6996-7003.

Wheate, N.J., Vora, V., Anthony, N.G., McInnes, F.J., 2010. Host-guest complexes of the antituberculosis drugs pyrazinamide and isoniazid with cucurbit [7] uril. *Journal of Inclusion Phenomena and Macrocyclic Chemistry* 68, 359-367.

Würflinger, A., 1975. Differential thermal analysis under high pressure IV: Low - temperature DTA of solid - solid and solid - liquid transitions of several hydrocarbons up to 3 kbar. *Berichte der Bunsengesellschaft für physikalische Chemie* 79, 1195-1201.

Zhang, K., Shen, H., Xu, S., Zhang, H., Zhu, M., Shi, P., Fu, X., Yang, Y., Gong, J., 2017. Thermodynamic study of solubility for pyrazinamide in ten solvents from T=(283.15 to 323.15) K. *The Journal of Chemical Thermodynamics* 112, 204-212.

Figure Captions

Figure 1. Molecular structure of pyrazinamide, molecular weight M is $123.11 \text{ g mol}^{-1}$

Figure 2. DSC curve (10 K min^{-1}) of commercial pyrazinamide form α transforming into γ at around 425 K , which melts at around 462 K (black line) and a DSC curve of a sample with a very large specific volume ($V_{\text{pan}}/m_{\text{PZA}}$) of which only the end of sublimation can be observed (449 K , red line). **Inset:** a close-up of the DSC curve of 0.01 mg illustrating the end of sublimation before the melting point of γ is reached. The extension of the baseline is indicated by the blue dotted line.

Figure 3. The enthalpy of fusion of form γ as a function of the specific volume available to PZA in the DSC capsule (see text). **Inset:** close-up on the evolution of the enthalpy of fusion at low specific volume. An upward curvature of the line at low specific volume can be observed.

Figure 4. Transition temperature of the α to γ transition obtained by DSC at different heating rates. No conclusive equilibrium temperature can be obtained from this behavior (equilibrium temperature from Table 4 indicated for reference).

Figure 5. (a) High-pressure differential thermal analysis curves, **(b)** The transition pressure of α to γ (■) and the melting pressure of γ (●) as a function of the temperature.

Figure 6. The X-ray diffraction patterns of pyrazinamide **(a)** form α and **(b)** form γ at different temperatures ($\lambda = 1.54056 \text{ \AA}$).

Figure 7. The specific volume of pyrazinamide form α and form γ at different temperatures. (■) α form this work, (●) γ form this work, (□) α form from the literature (A.Nangia and A.Srinivasulu, 2005; Battilocchio et al., 2014; Rajalakshmi et al., 2014; Takaki et al., 1960; Tiwari et al., 1980; Tiwari et al., 1982), (○) γ form from the literature (Castro et al., 2009; Cherukuvada et al., 2010; Nakata and Takaki, 1987; Tamura et al., 1961). The error bars for the data obtained in this work are smaller than the symbols.

Figure 8. The specific volumes of polymorphs α and γ as a function of pressure. (■) α form, (●) γ form at 295 K . The error bars are smaller than the symbols.

Figure 9. The solubility of polymorphs α and γ at different temperatures. (■) α (this work), (●) γ (this work), (▲) α obtained by Hermanto et al., (◆) α obtained by Zhang et al. (▼) γ

obtained by Hermanto et al. The error bars for the data obtained in this work are smaller than the symbols.

Figure 10. A sketch of the thermal expansion of the liquid in relation to the thermal expansion of the solids.

Figure 11. The two-panel pressure-temperature phase diagram of the α and γ polymorphs, the liquid, L, and the vapor phase, V. **High pressure panel (Top):** Two-phase equilibria: black (line + points (■)): α - γ , blue line: α -L, red (line + points (■)): γ -L. (●) is metastable triple point α - γ -L, (●) is stable triple point α - γ -V, (●) is metastable triple point α -L-V and (●) is stable triple point γ -L-V. **Low pressure panel (below):** Zoom on the vapor phase with orange line: L-V equilibrium, purple line: γ -L equilibrium and green line α -L equilibrium. Solid lines: stable equilibria, dashed lines: metastable equilibria, dotted lines: super-metastable equilibria. Solid circle: stable triple point, semi-solid circle: metastable triple point.

The phase relationship between the pyrazinamide polymorphs α and γ

Kangli Li¹, Gabin Gbabode¹, Maria Barrio², Josep-Lluís Tamarit², Marine Vergé-Depré³, Benoît Robert³, Ivo B. Rietveld^{1,4,*}

¹ Laboratoire SMS-EA3233, UFR des Sciences et Techniques, Université de Rouen Normandie, Place Emile Blondel, 76821 Mont-Saint-Aignan, France

² Grup de Caracterització de Materials, Departament de Física and Barcelona Research Center in Multiscale Science and Engineering, Universitat Politècnica de Catalunya, EEBE, Campus Diagonal-Besòs, Av. Eduard Maristany 10-14, E-08019 Barcelona, Catalonia, Spain

³ Sanofi R&D, Pharmaceuticals Development Platform/Analytical Sciences/Solid State Group, 13 quai Jules Guesde, F-94400 Vitry sur Seine, France

⁴ Faculté de Pharmacie, Université Paris Descartes, 4 avenue de l'observatoire, 75006 Paris, France

* Corresponding author: ivo.rietveld@univ-rouen.fr

Abstract

Pyrazinamide is an active pharmaceutical compound for the treatment of tuberculosis. It possesses at least four crystalline polymorphs. Polymorphism may cause solubility problems as the case of ritonavir has clearly demonstrated; however, polymorphs also provide opportunities to improve pharmaceutical formulations, in particular if the stable form is not very soluble. The four polymorphs of pyrazinamide constitute a rich system to investigate the usefulness of metastable forms and their stabilization. However, despite the existence of a number of papers on the polymorphism of pyrazinamide, well-defined equilibrium conditions between the polymorphs appear to be lacking. The main objectives of this paper are to establish the temperature and pressure equilibrium conditions between the so-called α and γ polymorphs of pyrazinamide, its liquid phase, and vapor phase and to determine the phase-change inequalities, such as enthalpies, entropies, and volume differences. The equilibrium temperature between α and γ was experimentally found at 392(1) K. Moreover, vapor pressures and solubilities of both phases have been determined, clearly indicating that form α is the more stable form at room temperature. High-pressure thermal analysis and the topological pressure-temperature phase diagram demonstrate that the γ form is stabilized by pressure and becomes stable at room temperature under a pressure of 260 MPa.

KEYWORDS

Vapor pressure, solubility, thermal expansion, solid-solid transition, specific volume, pressure-temperature phase diagram, active pharmaceutical ingredient

2. Introduction

5.1 Crystalline Polymorphism

Polymorphism is an aptitude of organic and inorganic compounds to crystallize in different crystal structures. Intermolecular interactions and free energies will be different for each crystal structure (Hilfiker, 2006). Thus, for applications that depend on consistency and stability, such as drugs, it is important to understand which of the possible forms is the most stable, and how to control the persistence of a formulation for a required amount of time in case the chosen form is not the more stable one. Changes in the crystal structure will affect the solubility and bioavailability of drugs (Censi and Di Martino, 2015), the crystal shape and flowability (Datta and Grant, 2004), and the crystal volume, which may cause formulations such as tablets to disintegrate (Su et al., 2018). Polymorph transformations can occur during storage or during processing like tableting or wet granulation (Brits et al., 2010; Morris et al., 2001). In this paper, the active pharmaceutical ingredient (API) pyrazinamide with at least four polymorphs, α , β , γ , and δ is investigated. The phase behavior of pyrazinamide will be discussed with a focus on the α and γ phases for which we present new data.

5.2 Literature data on the phase behavior of pyrazinamide

Pyrazinamide (PZA) is an API against tuberculosis and its molecular structure is shown in Figure 1. Forms Polymorphs α , β and γ are monoclinic, and their space groups are $P2_1/n$, $P2_1/c$ and Pc , respectively, whereas δ is triclinic and its space group is $P\bar{1}$ (A.Nangia and A.Srinivasulu, 2005; Battilocchio et al., 2014; Castro et al., 2009; Cherukuvada et al., 2010; Jarzemska et al., 2014; Nakata and Takaki, 1987; Rajalakshmi et al., 2014; Rø and Sørum, 1972a, b; Takaki et al., 1960; Tamura et al., 1961; Tiwari et al., 1980; Tiwari et al., 1982). Comparing the packing of the four forms, the α , β and δ forms contain head-to-head hydrogen bonded dimers between the amide groups. In the γ form, the molecules are arranged in catemers with hydrogen bonds linking the amide group with the top of the pyrazine ring. The γ polymorph exhibits disorder in which for about 20 % of the molecules the position of the ring and the amide group are inverted (Cherukuvada et al., 2010; Wahlberg et al., 2013).

Besides the polymorphs, a lot of crystallographic work has been carried out on mixtures of PZA with excipients or other APIs. Cocrystals containing pyrazinamide with carboxylic acids (Abourahma et al., 2015; Adalder et al., 2012; Kulla et al., 2016; Luo and Sun, 2013), with haloperfluorinated compounds (Choquesillo-Lazarte et al., 2017), with hydrochlorothiazide (Wang et al., 2014), with pyrogallol (Thakuria et al., 2012) and with diflunisal (Évora et al., 2011) have been described. Several polymorphs of cocrystals of PZA with succinic acid (Cherukuvada and Nangia, 2012; Luo and Sun, 2013), malonic acid (Kulla et al., 2017) and theophylline (Eddleston et al., 2015) have been found and investigated. Different binary mixtures leading to either cocrystals or eutectic systems have been described by Rajbongshi et al. (Rajbongshi et al., 2018). A ternary cocrystal has been designed by using a “drug-bridge-drug” strategy involving PZA combined with another first-line antitubercular drug isoniazid using fumaric acid as the bridge (Liu et al., 2018).

Calorimetric data available in the literature on the different polymorphs have been compiled in Table 1. The average melting temperature of form γ observed in the literature is 462(2) K² with very little variation in the data. The melting enthalpy exhibits a larger spread around the average value of 221(10) J g⁻¹, while the value of 177 J g⁻¹ has been omitted as a clear outlier. The average solid-solid transition temperature observed for α - γ is 421(4) K with an enthalpy of 11(4) J g⁻¹. However, Castro et al. carried out thorough investigations on the phase behavior of PZA using differential scanning calorimetry (DSC) and thermal stage microscopy, supported by X-ray powder diffraction (XRPD) and infrared spectroscopy and they observed that the α - γ transition depends on the heating rate of the DSC (Castro et al., 2009). This makes it rather doubtful that the average observed solid-solid transition temperature between α and γ is their equilibrium temperature. Cherukuvada et al. reported on polymorphic transition temperatures and enthalpies, relative stabilities and crystal structure data (at 100 K) (Cherukuvada et al., 2010). A schematic energy-temperature diagram was established resulting in the following stability hierarchy at room temperature $\alpha > \delta > \gamma > \beta$ with α the thermodynamically stable polymorph (Cherukuvada et al., 2010). Castro et al. reached a similar conclusion with the stability hierarchy of $\delta > \alpha > \gamma$ at low temperature, which may or may not include room temperature (Castro et al., 2009). γ is the stable form at high temperature in all references. The specific volume of different polymorphs of PZA in the literature is shown in Table 2.

Table 1. Calorimetric and crystallographic data of the different phase transitions of pyrazinamide in the literature^a

Transition	T/K	$\Delta H / J g^{-1}$	Heating rate /K min ⁻¹	References
$\gamma \rightarrow L$	461.4(5)	228(5)	10	(Castro et al., 2009)
	461.5(1)	228(3)	10	(E. Castro et al., 2011)
	461.8(2)	213(5)	5	(Cherukuvada et al., 2010)
	462.5(2)	220(5)	2	(Blokhina et al., 2015b)
	462.25	221.6	10	(Wheate et al., 2010)
	465.7(2)	220(5)	2	(Blokhina et al., 2015a)
	463.15		10	(Luo and Sun, 2013)
	461.15	177	10	(Lavor et al., 2012)
	461.4(5)	229(3)	5	(Lourenço et al., 2012)
	462.2(1)		10	(Pajula et al., 2010)
461.5(1)	217(24)	5	(Baaklini et al., 2015)	
	418.15-419.15			(Sharma et al., 2018)
$\alpha \rightarrow \gamma$	420.1(5)	13.2(7)	10	(Castro et al., 2009)
	428.25	10.6	5	(Cherukuvada et al., 2010)
	420.15	5	10	(Lavor et al., 2012)
	420.4(5)	13.3(2)	5	(Lourenço et al., 2012)
	420.65	11.35	5	(Baaklini et al., 2015)
$\delta \rightarrow \gamma$	408(5)	17(2)	10	(Castro et al., 2009)
	404.35	13.5	5	(Cherukuvada et al., 2010)

² The number in parentheses is the uncertainty in the last digit of the value, i.e. 1.23(4) equals 1.23 ± 0.04.

$\delta \rightarrow \alpha$	395(1)	$\Delta H > 0^b$	10	(Castro et al., 2009)
$\beta \rightarrow \gamma$	368.15	$\Delta H > 0^b$	10	(Castro et al., 2009)
	372.55	6.3	5	(Cherukuvada et al., 2010)
PZA \rightarrow vap		829(18) ^c		(Ribeiro da Silva et al., 2005)
$\alpha \rightarrow$ vap		915(13) ^d		(Blokhina et al., 2015a)
$\alpha \rightarrow$ vap		715(44) ^e		(Negoro, 1959; Negoro, 1960)

^a Values from the literature reported in °C or in J mol⁻¹ are adjusted by adding 273.15 K or are divided by 123.11 g mol⁻¹, respectively; an average value is used in this table when multiple values have been reported in the same paper; values are rounded to the number of reported digits in the respective reference.

^b Enthalpy values have not been mentioned in the reference (Castro et al., 2009), but DSC curves in the figures indicate endothermic transitions with increasing temperature.

^c Most likely form γ as the temperature of measurement is 421 K, however the enthalpy has been adjusted by the authors to the value expected at 298.15 K.

^d The temperature range is from 359.15 K to 383.15 K.

^e The temperature range is from 353.15 K to 383.15 K.

Table 2. Specific volume of different polymorphs of PZA in the literature

Polymorph	Space group	T/ K	V ^a / Å ³	Specific volume ^b / cm ³ g ⁻¹	References ^c
α	<i>P2₁/a</i>	RT ^d	567.518	0.69403	PYZIN (Takaki et al., 1960)
	<i>P2₁/c</i>	RT ^d	569.817	0.69684	PYZIN04 (Tiwari et al., 1980)
	<i>P2₁/a</i>	RT ^d	577.773	0.70657	PYZIN14 (Tiwari et al., 1982)
	<i>P2₁/n</i>	100	546.642	0.66850	PYZIN15 (A.Nangia and A.Srinivasulu, 2005)
	<i>P2₁/n</i>	180	554.291	0.67785	PYZIN21 (Battilocchio et al., 2014)
	<i>P2₁/n</i>	100	547.276	0.66927	PYZIN22 (Rajalakshmi et al., 2014)
β	<i>P2₁/c</i>	RT ^d	559.730	0.68450	PYZIN01 (Rø and Sørnum, 1972a)
	<i>P2₁/c</i>	90	540.881	0.66145	PYZIN23 (Jarzembska et al., 2014)
	<i>P2₁/c</i>	100	540.354	0.66081	PYZIN18 (Cherukuvada et al., 2010)
δ	<i>P$\bar{1}$</i>	RT ^d	279.557	0.68375	PYZIN02 (Rø and Sørnum, 1972b)

	$P\bar{1}$	100	268.818	0.65749	PYRZIN16 (A.Nangia and A.Srinivasulu, 2005)
	Pa	RT ^d	280.040	0.68493	PYRZIN03 (Tamura et al., 1961)
	Pa	RT ^d	275.136	0.67294	PYRZIN05 (Nakata and Takaki, 1987)
γ	Pc	293	275.917	0.67485	PYRZIN17 (Castro et al., 2009)
	Pc (with disorder) ^e	100	268.057	0.65562	PYRZIN19 (Cherukuvada et al., 2010)
	Pc (without disorder) ^f	100	267.226	0.65359	PYRZIN20 (Cherukuvada et al., 2010)

^aThe data is obtained from the CSD.

^bSpecific volume is calculated with the unit cell volume.

^cCSD reference code and literature reference.

^dRoom temperature: 283-303K.

^e Disorder taken into account.

^f Disorder not taken into account.

Including pressure into the analysis, Tan et al. found crystallographic indications that γ transforms into β at a pressure of about 4 GPa at room temperature (Tan et al., 2012). It implies that form β would be more stable than γ above 4 GPa. For α and δ , no transformations under pressure have been observed up to 13 GPa (Tan et al., 2012). Smets et al. investigated the transformation mechanism of PZA and concluded that the transition from the γ form to the low temperature δ and α forms include a vapor-mediated recrystallization process, while the transition from the low temperature forms to the γ form during heating included nucleation and growth within the crystal (Smets et al., 2018).

Because γ is a metastable form of PZA under ambient conditions, which is easily obtained through processing, it may be an interesting target to increase the bioavailability of PZA, although the polymorph does not persist for a long time under ambient conditions (Baaklini, 2015; Baaklini et al., 2015; Smets et al., 2018). Baaklini et al. have investigated polymorph control by spray drying with different additives and they managed to prevent spontaneous transformation of γ . They also found that the γ form persists at room temperature for several years by co-spray drying with 1,3-dimethylurea (Baaklini, 2015; Baaklini et al., 2015).

Pyrazinamide is prone to crystallize and the vitreous state is very difficult to reach. Borba et al. prepared the vitreous state by depositing vapor at 10 K and they observed recrystallisation into the δ phase at 260 K while heating (Borba et al., 2009), which is the closest observation to a glass transition temperature reported in the literature, if one assumes that PZA crystallizes immediately once it reaches T_g on heating the glass. Cooling crystallization from solution specifically targeting the δ form has been published by Hermanto et al. (Hermanto et al., 2015). Solubility of α , γ and δ in water and solubility of α in

four organic solvents and one mixture of solvents have been determined. The results showed that the solubility of PZA increases with increasing temperature and the solubility data in water from about 287 K to 316 K indicated the following ranking $x(\gamma) > x(\delta) > x(\alpha)$. Solubility of α in various solvents have been obtained by Zhang et al. (Zhang et al., 2017).

A number of modelling studies involving PZA have been published. The most extensive is that of Wahlberg et al. demonstrating and quantifying disorder in the structure of the γ form (Wahlberg et al., 2013) as mentioned before by Cherukuvada et al. (Cherukuvada et al., 2010). Computational studies specifically targeting the β form of pyrazinamide have been published by Jarzemska et al. (Jarzemska et al., 2014). The α - γ phase transformation has been investigated by in situ Raman and density functional theory (DFT) leading to a transition temperature of 418.15-419.15 K (Sharma et al., 2018). The four polymorphs of PZA have been studied by Hirshfeld surface and fingerprint plots (Luo et al., 2015).

A few studies have been published on vapor pressure of PZA. Blokhina et al. provided the vapor pressure as a function of the temperature from 359.15 K to 383.15 K: $\ln(P / \text{Pa}) = -13360(178) / T (\text{K}) + 38.3(5)$, which was verified to belong to the alpha phase (Blokhina et al., 2015a). Negoro et al. reported the vapor pressure of the α form as a function of temperature from 353.15 K to 383.15 K as well (Negoro, 1960). Ribeiro et al. obtained the vapor pressure of most likely the γ form, considering the measurement temperature, but the authors did not verify the polymorph under study (Ribeiro da Silva et al., 2005). The sublimation enthalpy values from the different vapor pressure measurements vary too much to draw any solid conclusions about the stability and the equilibrium temperature between the α and γ phases (Table 1).

5.3 Topological pressure-temperature phase diagrams

Pressure-temperature (P-T) phase diagrams provide information on the relative stability between crystalline polymorphs as a function of the thermodynamic variables, characteristic for the Gibbs energy function, temperature and pressure. Such phase diagrams can be obtained by direct measurement, but due to experimental limitations, it is often easier to use the Clapeyron equation (eq. 1) to complete the phase diagram (Barrio et al., 2017; Inès et al., 2013):

$$\frac{dP}{dT} = \frac{\Delta S}{\Delta V} = \frac{\Delta H}{T\Delta V} \quad (1)$$

in which, ΔS is the entropy change between the two phases, ΔH is the enthalpy change, ΔV represents the volume change, and T is the equilibrium temperature at which the enthalpy change has been obtained. Eq. 1 provides the slope of a two-phase equilibrium as a function of the temperature and the pressure and phase diagrams obtained through extrapolation are called topological phase diagrams, because the positions of the equilibria will be qualitatively correct, but the uncertainty over their position may be larger than in the case of experimentally obtained equilibrium information.

In this paper, the phase behavior of polymorphs α and γ of pyrazinamide is reported using

data from DSC, PXRD, synchrotron PXRD and High-Pressure Differential Thermal Analysis (HP-DTA). The melting temperature and enthalpy of γ have been reviewed and those of α have been determined. In addition, a thorough study of the α - γ transition temperature and enthalpy has been carried out. Specific volumes as a function of temperature and pressure of these two polymorphs have been obtained by XRPD. The melting equilibrium of γ and the transition between α and γ have been measured by HP-DTA. Finally, the vapor pressure and the solubility of the α and γ forms have been measured. All the data has been combined to build a topological phase diagram demonstrating the stability hierarchy of the two polymorphs as a function of pressure and temperature.

6. Materials and Methods

6.1 Pyrazinamide

Pyrazinamide was purchased from Sigma-Aldrich (France) and its purity is $\geq 97.5\%$ (GC). The commercial form was determined to be polymorph α by X-ray diffraction. Single crystals of α were obtained by sublimation. The γ form was obtained by heating the commercial sample above the α - γ transition temperature (see text), but it can also be obtained from spray drying. PXRD and DSC were used to verify the obtained polymorphs.

6.2 Crystal growth by sublimation

The sublimation experiments have been carried out with a cylindrical oven containing a linear array of six independently controlled heating elements. A glass tube with 0.1 g of PZA was placed in the oven under atmospheric pressure, while the set temperature ranged from 353 K to 403 K (± 0.5 K). Using the independent heating elements, various gradients along the glass tube were imposed. The time for sublimation experiments ranged from 2 days to 2 weeks. No significant decomposition took place during these experiments as confirmed by chromatographic measurements (See Figure S4).

6.3 High-resolution powder X-ray powder diffraction

High-resolution PXRD was used to determine the specific volumes of the α and γ forms as a function of the temperature. Powdered specimens were placed in capillaries of 0.5 mm diameter. The measurements were carried out with a vertically mounted INEL cylindrical position sensitive detector (CPS-120) and by using the Debye–Scherrer geometry. Monochromatic Cu- $K\alpha_1$ radiation (1.54056 Å) applying an asymmetrically focusing incident-beam curved germanium monochromator was used and diffraction intensities were registered over a 2θ range from 3.0° to 111.878° with a step size of 0.029° . The temperature was controlled by a liquid nitrogen 700 series Cryostream Cooler (Oxford Cryosystems). The PXRD patterns were refined by FullProf software to calculate the specific volumes (Rodriguez-Carvajal et al., 2005).

6.4 Synchrotron powder X-ray diffraction

The specific volumes of α and γ as a function of pressure at room temperature were obtained using PXRD data measured on the high-pressure diffraction beamline PSICHE at the synchrotron SOLEIL (Gif sur Yvette, France) using a focused monochromatic mode and a Ge solid state detector. High pressure was controlled with a membrane driven diamond anvil cell

with an upper pressure limit of 2 GPa. Silicon oil was used as pressure transmitting medium. NaCl was used as an internal reference to determine the pressure. The wavelength used for the experiments was 0.4859 Å. Pawley fit refinements were carried out using TOPAS-Academic V4.1 software.

6.5 Differential Scanning Calorimetry

The thermal behavior of PZA was studied by two different calorimeters: a TA Q100 thermal analyzer and a DSC 214 from Netzsch. Both use an inert atmosphere of nitrogen gas. Mercury, indium, tin, bismuth and zinc have been used to calibrate the DSC 214, whereas the TA Q100 has been calibrated by indium. The α - γ transition was studied using heating rates from 0.05 K min⁻¹ up to 200 K min⁻¹. The amount of material from 0.01 mg to 15 mg in the DSC capsule was varied to study the melting enthalpy of form γ as a function of the amount of material present in the DSC pan of which the volume is 45 μ L. It has been verified that decomposition was negligible during these DSC measurements (see Figure S4).

6.6 High-Pressure Differential Thermal Analysis (HP-DTA)

Transition temperatures as a function of pressure were measured by using a high-pressure differential thermal analyzer constructed in-house following the design by Würflinger (Würflinger, 1975). Therm 240 oil from Lauda was used as pressure-transmitting medium. PZA was mixed with Golden perfluorated liquid from Bioblock scientific to avoid the presence of air in the measurement pan, which may affect the thermodynamic equilibrium. DSC runs on the TA Q100 (see above) have been carried out to verify that the perfluorinated liquid is inert in the presence of PZA. The temperature range of the HP-DTA is 298 to 473 K, the pressure range is 0 to 250 MPa and the heating rate used in the measurement is 2 K min⁻¹.

6.7 Vapor pressure measurement

Vapor pressure measurements have been carried out isothermally in the temperature range 293.15 K - 383.15 K with a DVS Vacuum apparatus from Surface Measurements Systems, London, U.K., using a Knudsen cell whose orifice had a diameter of 440 micrometers and using benzoic acid vapor pressure as a standard.

6.8 Solubility measurement

The solubility in water of the α and γ forms of PZA has been measured in the range of 283.15 K to 313.15 K. A vial with water, which had been weighed, was placed in a jacketed crystallizer, while the temperature was controlled by a thermostat bath (CF41 Julabo). A predetermined mass of PZA weighed by a balance with a precision of 0.1 mg was added to the solution step by step. When the suspension remains visible in the solution for more than one hour, the solution was considered to be saturated. The final weight of PZA divided by the total amount of water is taken as the solubility at the set temperature.

7. Results

7.1 Calorimetric properties of the phase equilibria between α , γ , and the liquid

7.1.1 The melting equilibrium of form γ

A typical DSC curve of commercial PZA (form α) can be found in Figure 2. At a scanning rate of 10 K min^{-1} , α transforms into γ at around 425 K followed by the melting peak of γ at around 462 K (Figure 2). To determine the enthalpy and temperature of fusion of γ , measurements have been carried out at 10 K min^{-1} for a large number of samples of different mass. It became quickly clear that the enthalpy of fusion depends on the amount of material in the DSC capsule, similar to the cases of camphor (Rietveld et al., 2010) and adamantane (Espeau and Céolin, 2001). Therefore, the enthalpy of fusion was plotted as a function of the “specific volume” of the sample as shown in Figure 3 (the enthalpies and temperatures of fusion can be found in the supplementary materials Table S1). The “specific volume” of the sample in a DSC experiment ($V_{\text{pan}}/m_{\text{sample}}$) is the volume of a sealed DSC pan (V_{pan}), which includes its dead volume not taken up by solid PZA, divided by the mass of the weighed-in sample (m_{sample}). In most cases, when the vapor pressure of the solid is low, no consistent variation in the melting enthalpy will be observed; however, for pyrazinamide, a clear decrease of the measured specific enthalpy of fusion is observed with increasing “specific volume” (i.e. with decreasing mass, see Figure 3). The sublimation can in fact be observed by DSC, which is illustrated by two DSC curves of samples with a large difference in mass, as shown in Figure 2. The bottom curve exhibits a regular melting peak observed for a sample with a weight of 5.88 mg, whereas the top DSC curve represents a sample of 0.01 mg. In the inset, an upward shift from the baseline can be observed as a result of sublimation. Only a small peak-like drop to the baseline is observed at 449 K below the recorded melting temperature indicating that the sample has completely sublimated before it could have melted. Obviously, this rise of the baseline is also present in the curves with clear melting peaks, but in that case this baseline effect is dwarfed by the melting peak.

Taking the enthalpy data in Figure 3, one can establish a linear relationship with the specific volume in the DSC pan: $\Delta_{\gamma \rightarrow L}H (V_{\text{pan}}/m_{\text{sample}}) = -0.130(3) V_{\text{pan}}/m_{\text{sample}} + 236.1(9)$ leading to an enthalpy of fusion for a fully filled pan in the order of 236 J g^{-1} . However, it can be seen in the inset of Figure 3 that at the lowest specific volumes (i.e. fully filled DSC capsules), the enthalpy of fusion tends to even higher values in the order of 240 J g^{-1} . In fact, in the inset of Figure 3 at its lower range, one can observe a slight upward curvature in the line. For this reason, only the points up to a specific volume of $20 \text{ cm}^3 \text{ g}^{-1}$ have been used for the extrapolation, leading to the expression for the melting enthalpy, $\Delta_{\gamma \rightarrow L}H (\text{J g}^{-1})$, as a function of the “specific volume”, $V_{\text{pan}}/m_{\text{sample}} (\text{cm}^3 \text{ g}^{-1})$: $\Delta_{\gamma \rightarrow L}H (V_{\text{pan}}/m_{\text{sample}}) = -0.623(10) V_{\text{pan}}/m_{\text{sample}} + 241.0(1.0)$. Extrapolating this line to the specific volume of the γ form at its melting temperature (this translates to a capsule filled entirely with PZA without dead volume and is equal to $0.7003(31) \text{ cm}^3 \text{ g}^{-1}$ as reported below) leads to an enthalpy of fusion of $240.6(1.0) \text{ J g}^{-1}$.

Considering the scatter over the enthalpy of fusion of form γ , the enthalpies and temperatures of fusion of three single crystals have been determined too; in particular because the surface to bulk ratio is much smaller than in the case of powder, it may diminish the effect of sublimation. The data can be found in Table 3; there is still a considerable scatter over the melting enthalpy data and it is not clear whether the relation between the weighed-in mass and the enthalpy (Table 3) is accidental or not, but the average of $240(5) \text{ J g}^{-1}$ confirms the results obtained with capsules tightly filled with powder.

The overall behavior of the melting enthalpy increasing with an increasing amount of PZA is

clearly caused by the tendency of PZA to sublime as is shown in Figure 2. Less clear is the observation that at very high loads, the enthalpy appears to curve slightly upwards, confirmed by both completely filled capsules and single crystal data. How this curvature comes about with powder samples could be explained by a combination of sublimation and disorder reported for the γ form (Cherukuvada et al., 2010; Wahlberg et al., 2013).

The melting temperature, which does not vary with sample mass, is much easier to determine. The average over 27 points is equal to 462.0(5) K ($n = 27$). This value is in accordance with the literature data (see Table 1).

Table 3. The melting point and the enthalpy of fusion of single crystals of polymorphs α and γ measured by DSC^a

Sample	α			γ		
	T_{fus}/ K	$\Delta H/ \text{J g}^{-1}$	m / mg	T_{fus}/ K	$\Delta H/ \text{J g}^{-1}$	m / mg
1	457.05	250.6	0.98	462.35	244	2.69
2	456.65	255.7	0.66	462.55	239.9	2.12
3				462.65	235.9	1.69
Average	457(1)	253(4)		462.5(5)	240(5)	

^a heating rate is 100 K min⁻¹.

7.1.2 The melting transition of form α

The temperature and enthalpy of fusion of form α have been obtained using single crystals subjected to DSC runs at 100 K min⁻¹ (See Table 3). The high scanning rate was necessary to outrun the solid-solid transition from α to γ . The DSC has been specially calibrated for these measurements at 100 K min⁻¹ with the four calibrants listed for the DSC 214 from Netzsch (see experimental section). The melting point is found at 457(1) K and the enthalpy of fusion equals 253(4) J g⁻¹. It was not possible to investigate the influence of sublimation on the melting properties of α , due to the inaccuracy of the DSC at 100 K min⁻¹ and because changing to smaller crystals would cause them to turn into γ before melting. However, the high scanning speed and the fact that the sample was a single crystal, which decreases the surface to bulk ratio, may have limited the effect of sublimation considerably.

7.1.3 The α - γ equilibrium temperature

The transition temperature of α to γ had been previously shown to depend on the heating rate of the DSC (Castro et al., 2009). However, the value at infinitely low heating rate remains unknown. In the current study, once again different heating rates have been used to investigate the temperature of conversion of form α into γ and the results are presented in Figure 4 (the values can be found in the supplementary materials in Table S2). It is clear from Figure 4 that the transition temperature decreases with decreasing heating rate and there is no visible levelling off at very low heating rates even if the values observed are still lower than those reported by Castro et al. (Castro et al., 2009). DSC appears not to be the most appropriate method to determine the transition temperature between forms α and γ due to this particular kinetic behavior of the transition. Therefore, each polymorph has been kept in an oven in separate experiments at a decreasing series of temperatures starting roughly at the lowest transition temperature observed by DSC. The results are presented in Table 4. It

can be seen that at 392 K initial form α turns into form γ . Moreover, subjecting γ to a temperature of 391 K, a single crystal of form α is grown, while at 390 K, several α crystals can be observed. It can be concluded that the most likely equilibrium temperature between α and γ can be found between 391 and 392 K. Lacking any further precision, the average between these values will be rounded off to the nearest digit: $T_{\alpha \rightarrow \gamma} = 392(1)$ K.

Table 4. The stability of the polymorphs α and γ at constant temperature

T/ K	Initial polymorph	Final polymorph	Comments
403	α	γ	
398	α	γ	
394	α	γ	
392	α	$\gamma + \alpha$	γ is single crystal
391	γ	$\gamma + \alpha$	One single crystal of α
390	γ	$\gamma + \alpha$	Few crystals of α
373	γ	α	
353	γ	α	

The enthalpy change associated to the α - γ transition has been determined at a scanning rate of 10 K min^{-1} . It did not depend on the sample mass as in the case of the melting point of γ , most likely because the lower temperature did not cause as much sublimation. Interestingly, the enthalpy difference between the two polymorphs remained constant even if the transition temperature ranged from 405 to 440 K (the data can be found in the supplementary materials, Table S2 and Figure S1). The average of the α - γ transition enthalpy has been found to be $\Delta_{\alpha \rightarrow \gamma}H = 13.2(6) \text{ J g}^{-1}$ ($n = 83$).

The constant transition enthalpy between α and γ indicates that their difference in heat capacity does not change with the temperature. It also implies that the sum of the enthalpies of the cycle α to γ to liquid to α must be more or less equal to zero: $\Delta_{\alpha \rightarrow \gamma}H + \Delta_{\gamma \rightarrow L}H - \Delta_{\alpha \rightarrow L}H = 13.2 + 240 - 253 = 0.2 \cong 0$. The fact that this sum indeed equals zero indicates that the enthalpy differences between phases α , γ , and the liquid appear to be consistent. One may therefore conclude that most likely the enthalpy difference between α and γ is temperature independent between their equilibrium temperature and the melting point of PZA. The value is equal to the values reported in literature (Castro et al., 2009; Lourenço et al., 2012). However, the transition temperature between the two solids at 392 K appears to be at least 20 degrees lower, than previously reported in the literature (Table 1) (Castro et al., 2009).

7.1.4 The glass transition of pyrazinamide

In principle, the glassy state of a chemical compound can be obtained by quenching its melt. However, PZA is not a good glass former and it recrystallizes rapidly even if quenched in liquid nitrogen after melting. Therefore, it has been difficult to obtain conclusive results on the temperature of the glass transition. However, in most measurements, a departure from the baseline, indicating the occurrence of a phase transition and thus the presence of molecular mobility, could be observed between 250 and 260 K in accordance with the paper

of Borba et al, who observed the formation of δ from glassy film at 260 K (Borba et al., 2009). It seems therefore appropriate to set the glass transition temperature at 260 K as the highest possible estimate.

7.1.5 The α - γ transition and the fusion of γ under pressure

High-pressure differential thermal analysis curves containing the peaks for the α to γ transition and the fusion of γ are shown in Figure 5a. The observed transitions have been plotted as a function of the pressure and the temperature and are presented in Figure 5b. The values can be found in the supplementary materials (fusion of γ : Table S3 and the α - γ transition: Table S4). The solid-solid transition was difficult to measure and only a few points could be obtained. In both cases the data has been fitted to a straight line in the form of the pressure P /MPa as a function of the temperature T /K:

$$\gamma \rightarrow L: P = 3.5(3) T - 1623(100) \quad (2)$$

$$\alpha \rightarrow \gamma: P = -3.6(7) T + 1510(283) \quad (3)$$

7.2 The specific volumes of polymorphs α and γ

7.2.1 Temperature dependence of the specific volume

The specific volumes of forms α and γ as a function of the temperature have been obtained by high-resolution PXRD. The X-ray diffraction patterns are provided in Figure 6 and the resulting specific volumes are presented in Figure 7 (the values can be found in the supplementary materials Table S5). The data has been fitted to the following expressions of specific volume V_i ($\text{cm}^3 \text{g}^{-1}$) as a function of the temperature T (K):

$$V_\alpha = 0.6624(7) + 6.8(6) \times 10^{-5} T + 8.44 (1.06) \times 10^{-8} T^2 \quad (4)$$

$$V_\gamma = 0.6520(7) + 4.8(5) \times 10^{-5} T + 1.22(9) \times 10^{-7} T^2 \quad (5)$$

Comparing the specific volume of form α and γ measured in this work and the literature (see Figure 7), the specific volume of form α is larger than that of form γ : $V_\alpha > V_\gamma$. In other words, the density of α is smaller than that of form γ : $d_\alpha < d_\gamma$. Interestingly, the difference in specific volume hardly changes from 100 K up to 400 K: $\Delta_{\alpha \rightarrow \gamma} V(T) = -0.01242(23) - 1.1(9) \times 10^{-6} T$ and the average difference in volume between α and γ is $\Delta_{\alpha \rightarrow \gamma} V = -0.0127(4) \text{ cm}^3 \text{g}^{-1}$ with an error of less than 2.5 % (see also Figure 7). Although the literature data appears to be somewhat scattered in Figure 7, the γ form is clearly the denser one.

7.2.2 Pressure dependence of the specific volume

The powder diffraction patterns obtained under different pressures at 295 K can be found in the supplementary materials (Figure S2 and S3) and the values of the specific volumes as a function of pressure obtained from the patterns have been reported in Table S6 and are also depicted in Figure 8. The specific volumes V_i ($\text{cm}^3 \text{g}^{-1}$) of forms α and γ have been expressed as a function of the pressure P /MPa in the following two equations:

$$V_{\alpha} = 0.6883(2) - 5.27(4) \times 10^{-5} P + 9.0(2) \times 10^{-9} P^2 \quad (6)$$

$$V_{\gamma} = 0.6826(6) - 5.17(12) \times 10^{-5} P + 8.5(6) \times 10^{-9} P^2 \quad (7)$$

The specific volumes of the two forms decrease with increasing pressure while form γ is denser than form α as expected from the results shown just above. It can be seen that eqs. 6 and 7 are very similar. Using a 3rd order Birch-Murnaghan equation of state (see the Supplementary Materials for the equation) (Angel et al., 2014a; Angel et al., 2014b; Birch, 1947) a measure for the compressibility can be obtained, which leads for α to a specific volume at 0 MPa and 295 K $V_{0,295\text{ K}} = 0.6891(2) \text{ cm}^3 \text{ g}^{-1}$, a bulk modulus (i.e. inverse compressibility) $K_{0,295\text{ K}} = 11.1(2) \times 10^3 \text{ MPa}$ and its derivative with pressure of $K'_{0,295\text{ K}} = 9.8(3)$. For γ , the results are: $V_{0,295\text{ K}} = 0.6869(2) \text{ cm}^3 \text{ g}^{-1}$, $K_{0,295\text{ K}} = 9.30(4) \times 10^3 \text{ MPa}$ and $K'_{0,295\text{ K}} = 12.1(1)$. The bulk moduli and derivatives of the two polymorphs are similar.

7.3 The vapor pressure of the α and γ polymorphs

A few papers contain data on the vapor pressure of the α form (Blokhina et al., 2015a; Negoro, 1959; Negoro, 1960), however, data obtained by different methods are difficult to compare. Thus, the vapor pressure of α and γ as a function of the temperature is measured in this work with the same equipment and the result is shown in Table S7. Using the Clausius–Clapeyron equation ($\ln P = -\Delta_{S \rightarrow V}H/RT + B$, $\Delta_{S \rightarrow V}H$ is the enthalpy of sublimation, B is a constant), the vapor pressure $P(\text{Pa})$ can be expressed as a function of the temperature $T(\text{K})$:

$$\alpha \rightarrow V: \ln P = -94945(1024) / RT + 32.3(4) \quad (R^2 = 0.9991) \quad (8)$$

$$\gamma \rightarrow V: \ln P = -92192(2024) / RT + 31.5(7) \quad (R^2 = 0.9986) \quad (9)$$

with the numerator the enthalpy of sublimation in J mol^{-1} and R the gas constant, $8.3145 \text{ J K}^{-1} \text{ mol}^{-1}$. The sublimation enthalpies from eqs. 8 and 9 reflect the differences in enthalpy between the respective polymorph and the vapor phase. It implies that the difference between these two enthalpies must be similar to the transition enthalpy between the two solid phases: $\Delta_{\alpha \rightarrow \gamma}H = \Delta_{\alpha \rightarrow V}H - \Delta_{\gamma \rightarrow V}H = 94945 - 92192 = 2.75(2.27) \text{ kJ mol}^{-1}$ or $22(19) \text{ J g}^{-1}$. Obviously, the error over the large enthalpy values is considerable, which is reflected in the large error over the transition enthalpy of 19 J g^{-1} ; however, the value is equal within error with that of the DSC even if the vapor pressure is simply not precise enough to determine an accurate enthalpy difference. In comparison with the literature values (Table 1), the enthalpies of vaporization found here, 771 J g^{-1} for α and 749 J g^{-1} for γ , are similar; however, the spread in the values in Table 1 is large and it seems essential that data for different polymorphs are obtained with a single apparatus for reliable comparison.

The intersection between the two lines eqs. 8 and 9, where the vapor pressure of the two polymorphs is equal, should coincide with the equilibrium temperature for α and γ . It is found at about 398 K, which is somewhat higher than 392 K, the result obtained in Table 4.

7.4 The solubility of α and γ

The solubilities in water of the α and γ polymorphs measured at different temperatures and those found in the literature (Hermanto et al., 2015; Zhang et al., 2017) are provided in Table S8 and Figure 9. The solubility of γ is higher than the solubility of α . The solubility of α measured in this work is similar to the data measured in the literature, but the solubility of γ is different. This may be explained by the metastability of γ , which may cause a larger error over the result due to stability issues. The solubility data can be fitted using the van't Hoff equation:

$$\ln x_i = -\frac{\Delta_{d(i)}H}{RT} + \frac{\Delta_{d(i)}S}{R} \quad (10)$$

where x_i is the mole fraction solubility of form i (/mmol mol⁻¹), $\Delta_{d(i)}H$ and $\Delta_{d(i)}S$ represent the dissolution enthalpy and entropy of form i in water, respectively. T is the temperature (/K), and R is the gas constant.

$$\alpha: \ln x = -28917(643) / RT + 12.5(3) \quad (R^2 = 0.9985) \quad (11)$$

$$\gamma: \ln x = -26714(1034) / RT + 11.7(5) \quad (R^2 = 0.9955) \quad (12)$$

Like the enthalpy of sublimation, the transition enthalpy can be calculated: $\Delta_{\alpha \rightarrow \gamma}H = \Delta_{d(\alpha)}H - \Delta_{d(\gamma)}H = 28.917 - 26.714 = 2.21(1.3)$ kJ mol⁻¹ or 18 (10) J g⁻¹. Errors are again large due to the comparison between two large values; however, the overall difference in enthalpy between the two polymorphs is close to the value of 13.2 J g⁻¹ obtained by DSC. The equilibrium transition temperature between α and γ in the presence of water can be calculated using eq. 11 and 12, the intersection of these two lines being the transition temperature. It is found at 330(4) K. This temperature is lower than that obtained through the oven and the vapor pressure experiments. This could be due to the difficulties in interpreting the solubility data due to metastability and the interaction between solvent and solute, which may affect the chemical potentials of the polymorphs as described by the Gibbs-Duhem equation.

8. Discussion

8.1 Interpretation of the phase behavior of polymorphs α , γ , and the liquid

Using the data presented above, a pressure-temperature phase diagram can be constructed describing the behavior of the three condensed phases that have been investigated. Eq. 2 describes the pressure-temperature behavior of the melting equilibrium of γ . Considering that this transition is observed in the direction of a solid-liquid transformation and thus no significant kinetic barrier exists for the transition, there is little doubt that the obtained equation reflects the equilibrium behavior within error.

The same cannot be said about the α - γ transition, as is very clear from Figure 4, where the transition temperature decreases as the heating rate decreases. This implies that eq. 3, $P(T)_{\alpha \rightarrow \gamma}$, should be shifted to lower temperatures assuming that the slope will stay the same. In fact, the slope of the α - γ equilibrium can be verified with the Clapeyron equation (eq. 1), using the calorimetric and volumetric data discussed above: $T_{\alpha \rightarrow \gamma} = 392(1)$ K, $\Delta_{\alpha \rightarrow \gamma}H = 13.2(6)$

J g^{-1} , and with eqs. 4 and 5 $\Delta_{\alpha \rightarrow \gamma} v (392 \text{ K}) = -0.0124 (38) \text{ cm}^3 \text{g}^{-1}$, as $v_{\alpha} (392 \text{ K}) = 0.7021(29) \text{ cm}^3 \text{g}^{-1}$ and $v_{\gamma} (392 \text{ K}) = 0.6897(25) \text{ cm}^3 \text{g}^{-1}$. This leads to a slope of $-2.7(9) \text{ MPa K}^{-1}$. Even if the values of the slopes ($-3.6(7) \text{ MPa K}^{-1}$ in eq. 3) overlap within error, it is most likely that the slope of the α - γ equilibrium is closer to -2.7 MPa K^{-1} , because the transition points obtained by HP-DTA may suffer an overestimation in temperature as observed in the regular DSC measurements for this solid-solid transition. Thus, the pressure (P/ MPa) of the α - γ equilibrium can be expressed as a function of the temperature (T/ K) in the following adjusted way:

$$\alpha \rightarrow \gamma: P = -2.7(9) T + 1064(327) \quad (13)$$

In which the line is shifted to pass through 392 K at 0 MPa (representing the vapor pressure of PZA).

Taking the intersection of eqs. 2 and 13, one finds the triple point where the phases α , γ , and the liquid are in equilibrium, leading to 431 K and -105 MPa . Using this triple point in turn with the melting temperature of form α , 457 K at 0 MPa, the pressure (P/ MPa) for the melting equilibrium of form α as a function of temperature (T/ K) can be obtained:

$$\alpha \rightarrow \text{L}: P = 4.0 T - 1823 \quad (14)$$

It can be seen that this melting equilibrium is the steepest in the phase diagram as expected for the three diverging equilibria, α - γ , α -L, and γ -L, with increasing pressure.

8.2 The volume difference between solid and liquid on melting

For statistical reasons, it is of interest to study the change in the specific volume of the melting solid. In particular for cases for which it is not possible to have experimental access to the slope of the melting equilibrium using statistical data, an estimate of the slope can be obtained and a topological phase diagram can be constructed through thermodynamic reasoning.

In the case of pyrazinamide, the slope of the melting of the γ phase has been found to be $3.5 (3) \text{ MPa K}^{-1}$ (eq. 2) based on the HP-DTA data. Taking the melting enthalpy of $240(5) \text{ J g}^{-1}$ obtained above, the melting temperature of $462.0(5) \text{ K}$ and the specific volume of the γ form at the melting temperature (eq. 5), $V_{\gamma} (462.0 \text{ K}) = 0.7003(31) \text{ cm}^3 \text{g}^{-1}$, one obtains through the Clapeyron equation the volume change on melting, $\Delta_{\gamma \rightarrow \text{L}} V = 0.1473(92) \text{ cm}^3 \text{g}^{-1}$, and the specific volume of the liquid at the melting point: $V_{\text{L}} (462.0 \text{ K}) = 0.8476(97) \text{ cm}^3 \text{g}^{-1}$.

For the melting of the α form, information on the thermal expansion of the liquid can be used. From the results in this paper and from those of Borba, it can be concluded that the glass transition temperature can be found around 260 K (Borba et al., 2010). Because at the glass transition, the liquid turns into a glass, by approximation its density can be set equal to that of the least dense polymorph of pyrazinamide, which is form α (see Figure 7). At 260 K, form α will have a specific volume of $V_{\alpha} (260 \text{ K}) = 0.6858 \text{ cm}^3 \text{g}^{-1}$ (eq. 4). With the specific volume of the liquid at the melting point of the γ form, the specific volume of the liquid ($V_{\text{L}}/ \text{cm}^3 \text{g}^{-1}$) as a function of the temperature (T/ K) can be described by a straight line (seen Figure 10):

$$V_L = 0.47756 + 8.0101 \times 10^{-4}T \quad (15)$$

Using the known data on the melting of the α form, $T_{\alpha \rightarrow L} = 457(1)$ K, $\Delta_{\alpha \rightarrow L}H = 253(4)$ J g⁻¹, $V_{\alpha}(T_{\alpha \rightarrow L}) = 0.7112(35)$ cm³ g⁻¹ and $V_L(T_{\alpha \rightarrow L}) = 0.8435(3)$ cm³ g⁻¹ a change in the volume on the melting of α can be determined $\Delta_{\alpha \rightarrow L}V = 0.1323(36)$ cm³ g⁻¹. This leads to a slope for the melting equilibrium of 4.2(2) MPa K⁻¹. Comparing this to the slope in eq. 14 of 4.0 MPa K⁻¹, which has been obtained by extrapolation of the γ -L equilibrium and the α - γ equilibrium, demonstrates the strength of the topological method and the redundancy in the data due to the thermodynamic requirements they need to fulfill.

The ratio of the volume of the liquid by that of the solid form which melts is $V_L/V_{\gamma} = 1.21$ for γ and $V_L/V_{\alpha} = 1.19$ for α . These values are large in comparison with most small organic molecules and only form III of piracetam with a ratio of 1.18 comes anywhere near these values (Toscani et al., 2016). Goodman et al. (Goodman et al., 2004) found an average expansion on melting of about 12% for small organic molecules based on 21 compounds. Based on different distributions of small pharmaceutical molecules, similar expansions with an average in the order of 11% have been recorded (Céolin and Rietveld, 2015; Gavezzotti, 2007). The reason for the large difference in the specific volume between the solid state and the liquid state must lie in the flatness of the molecule, which makes efficient stacking possible in the solid, but which is obviously lost in the liquid state. The density of the γ form is indeed rather high for an organic substance with 1.43 g cm⁻³ at its melting point and 1.48 g cm⁻³ at room temperature.

8.3 The pressure-temperature phase diagram

The resulting topological pressure-temperature phase diagram of α - γ -L-V is presented in Figure 11. This phase diagram is built based on eqs. 2, 13, and 14 for the condensed phases and eqs. 8 and 9 for the vapor phases. The final liquid – vapor (L-V) equilibrium curve can be calculated as follows. The enthalpy of vaporization is $\Delta_{L \rightarrow V}H = \Delta_{\gamma \rightarrow V}H - \Delta_{\gamma \rightarrow L}H$; $\Delta_{\gamma \rightarrow V}H$ can be obtained from eq. 12 and amounts to 749(17) J g⁻¹ and $\Delta_{\gamma \rightarrow L}H$ is 240(5) J g⁻¹, so that $\Delta_{L \rightarrow V}H$ is 509(17) J g⁻¹. Eqs. 2 and 9 can be used to calculate the triple point of γ -L-V through which the L-V equilibrium curve must pass leading to the expression:

$$L \rightarrow V: \ln P = -7535 / T + 23.8 \quad (16)$$

with P in Pa and T in K.

9. Conclusions

This paper gives a clear demonstration of the fact that it can be very hard to obtain equilibrium data for molecular systems. The API Pyrazinamide suffers multiple problems: disorder in the high-temperature form, a high sublimation pressure at high temperatures, and extremely slow solid-solid phase transformations between almost all solid forms.

The high vapor pressure of pyrazinamide at elevated temperatures affects the melting enthalpy as demonstrated in Figure 3. In principle such behavior can be compensated by measurements that take the volume available to the sample into account as has been done

in this paper. Only single crystals and fully packed DSC capsules appear to approach the ideal melting enthalpy.

Extremely slow solid-solid transitions are nothing new for researchers working with differential calorimetry, however, finding the proper transition temperature with a transition that is found at ever lower temperatures when decreasing the scanning rate of the DSC is not an easy endeavor (Barrio et al., 2012; Rietveld et al., 2011). In the present case, only measurements outside of the DSC, e.g. heating samples in an oven for weeks appears to have provided a clue on where to find the solid-solid equilibrium between α and γ forms. Whether this approach will deliver any equilibrium temperatures in relation to the other solid forms is absolutely not clear yet. The data on vapor pressure and solubility confirm the equilibrium temperature; however, extrapolation and the errors over the vapor pressure and solubility data give rise to a rather large error margin.

The pressure-temperature phase diagram presented in Figure 11 only contains the two most studied phases of pyrazinamide, because equilibrium data on the other two forms β and δ still remain elusive due to the slow phase transition rates. In previous papers on the subject, no convincing evidence has been provided that equilibrium data on these two forms has been reported, leaving any conclusions on the stability of these two forms pending. Nonetheless, the present phase diagram involving the equilibria between α , γ , and the liquid remains valid, within the limits of the precision of the data, regardless of the stability hierarchy in relation to the other two solid phases. It is therefore clear, that from the point of view of form α , form γ is a high-pressure, high-temperature form, which under ambient temperature becomes stable at a pressure in the order of 260 MPa. This value is not high from a processing point of view, in particular if one considers that the equilibrium pressure will decrease with increasing temperature. Nonetheless, no α - γ transition has been observed under pressures up to 2 GPa in line with the observation that transition rates are very slow.

Declaration of Interests

The authors declare no competing financial interests

Acknowledgements

K. Li thanks the ERASMUS organization for a travel grant for three months of research in Barcelona. The authors thank Jean-Paul Itié for his support on beamline Psiché, synchrotron Soleil (Gif sur Yvette).

Funding: This work was supported by the Region Normandie, synchrotron Soleil (beamline Psiché), MINECO Project No. FIS2017-82625-P, and AGAUR DGU Project No. 2017SGR-42

References

- A.Nangia, A.Srinivasulu, 2005. CSD Communication (Private Communication)
- Abourahma, H., Shah, D.D., Melendez, J., Johnson, E.J., Holman, K.T., 2015. A Tale of Two Stoichiometrically Diverse Cocrystals. *Crystal Growth & Design* 15, 3101-3104.

Adalder, T.K., Sankolli, R., Dastidar, P., 2012. Homo-or heterosynthon? A crystallographic study on a series of new cocrystals derived from pyrazinecarboxamide and various carboxylic acids equipped with additional hydrogen bonding sites. *Crystal Growth & Design* 12, 2533-2542.

Angel, R.J., Gonzalez-Platas, J., Alvaro, M., 2014a. EosFit7c and a Fortran module (library) for equation of state calculations. *Z Krist-Cryst Mater* 229, 405-419.

Angel, R.J., Mazzucchelli, M.L., Alvaro, M., Nimis, P., Nestola, F., 2014b. Geobarometry from host-inclusion systems: The role of elastic relaxation. *Am. Mineral.* 99, 2146-2149.

Baaklini, G., 2015. Les Effets du Spray Drying sur le polymorphisme des composés pharmaceutiques et organiques. Rouen.

Baaklini, G., Dupray, V., Coquerel, G., 2015. Inhibition of the spontaneous polymorphic transition of pyrazinamide γ form at room temperature by co-spray drying with 1, 3-dimethylurea. *International journal of pharmaceutics* 479, 163-170.

Barrio, M., Maccaroni, E., Rietveld, I.B., Malpezzi, L., Masciocchi, N., Céolin, R., Tamarit, J.I., 2012. Pressure-temperature state diagram for the phase relationships between benfluorex hydrochloride forms I and II: a case of enantiotropic behavior. *Journal of pharmaceutical sciences* 101, 1073-1078.

Barrio, M., Tamarit, J.L., Ceolin, R., Robert, B., Guéchet, C., Teulon, J.M., Rietveld, I.B., 2017. Experimental and topological determination of the pressure-temperature phase diagram of morniflumate, a pharmaceutical ingredient with anti-inflammatory properties. *Journal of Chemical Thermodynamics* 112, S0021961417301544.

Battilocchio, C., Hawkins, J.M., Ley, S.V., 2014. Mild and selective heterogeneous catalytic hydration of nitriles to amides by flowing through manganese dioxide. *Organic letters* 16, 1060-1063.

Birch, F., 1947. Finite Elastic Strain of Cubic Crystals. *Phys. Rev.* 71, 809-824.

Blokhina, S., Sharapova, A., Ol'khovich, M., Volkova, T., Perlovich, G., 2015a. Vapor pressures and thermodynamic sublimation of antitubercular drugs. *J. Therm. Anal. Calorim.* 120, 1053-1060.

Blokhina, S.V., Ol'khovich, M.V., Sharapova, A.V., Volkova, T.V., Perlovich, G.L., 2015b. Solution thermodynamics of pyrazinamide, isoniazid, and p-aminobenzoic acid in buffers and octanol. *The Journal of Chemical Thermodynamics* 91, 396-403.

Borba, A., Albrecht, M., Gomez-Zavaglia, A., Suhm, M.A., Fausto, R., 2010. Low Temperature Infrared Spectroscopy Study of Pyrazinamide: From the Isolated Monomer to the Stable Low Temperature Crystalline Phase. *J. Phys. Chem. A* 114, 151-161.

Borba, A., Albrecht, M., Gómez-Zavaglia, A., Suhm, M.A., Fausto, R., 2009. Low temperature infrared spectroscopy study of pyrazinamide: from the isolated monomer to the stable low temperature crystalline phase. *The Journal of Physical Chemistry A* 114, 151-161.

Brits, M., Liebenberg, W., De Villiers, M.M., 2010. Characterization of polymorph transformations that decrease the stability of tablets containing the WHO essential drug mebendazole. *Journal of pharmaceutical sciences* 99, 1138-1151.

Castro, R.A., Maria, T.M., Évora, A.O., Feiteira, J.C., Silva, M.R., Beja, A.M., Canotilho, J., Eusébio, M.E.S., 2009. A new insight into pyrazinamide polymorphic forms and their thermodynamic relationships. *Crystal Growth & Design* 10, 274-282.

Censi, R., Di Martino, P., 2015. Polymorph impact on the bioavailability and stability of poorly soluble drugs. *Molecules* 20, 18759-18776.

Céolin, R., Rietveld, I.B., 2015. The topological pressure-temperature phase diagram of ritonavir, an extraordinary case of crystalline dimorphism. *Annales Pharmaceutiques Françaises* 73, 22-30.

Cherukuvada, S., Nangia, A., 2012. Fast dissolving eutectic compositions of two anti-tubercular drugs. *CrystEngComm* 14, 2579-2588.

Cherukuvada, S., Thakuria, R., Nangia, A., 2010. Pyrazinamide polymorphs: relative stability and vibrational spectroscopy. *Crystal Growth & Design* 10, 3931-3941.

Choquesillo-Lazarte, D., Nemec, V., Cinčić, D., 2017. Halogen bonded cocrystals of active pharmaceutical ingredients: pyrazinamide, lidocaine and pentoxifylline in combination with haloperfluorinated compounds. *CrystEngComm* 19, 5293-5299.

Datta, S., Grant, D.J., 2004. Crystal structures of drugs: advances in determination, prediction and engineering. *Nature Reviews Drug Discovery* 3, 42.

E. Castro, R.A., Ribeiro, J.D., Maria, T.M., Ramos Silva, M., Yuste-Vivas, C., Canotilho, J., Eusébio, M.E.S., 2011. Naproxen cocrystals with pyridinecarboxamide isomers. *Crystal Growth & Design* 11, 5396-5404.

Eddleston, M.D., Arhangelkis, M., Fabian, L., Tizzard, G.J., Coles, S.J., Jones, W., 2015. Investigation of an amide-pseudo amide hydrogen bonding motif within a series of theophylline: amide cocrystals. *Crystal Growth & Design* 16, 51-58.

Espeau, P., Céolin, R., 2001. Thermodynamic studies of solids with non-negligible vapour pressure: T–v and p–T diagrams of the dimorphism of adamantane. *Thermochimica acta* 376, 147-154.

Évora, A.O., Castro, R.A., Maria, T.M., Rosado, M.T., Ramos Silva, M., Matos Beja, A., Canotilho, J., Eusébio, M.E.S., 2011. Pyrazinamide-diflunisal: a new dual-drug co-crystal. *Crystal Growth & Design* 11, 4780-4788.

Gavezzotti, A., 2007. *Molecular aggregation: structure analysis and molecular simulation of crystals and liquids.* , OUP Oxford.

Goodman, B.T., Wilding, W.V., Oscarson, J.L., Rowley, R.L., Goodman, B.T., Wilding, W.V., Oscarson, J.L., Rowley, R.L., 2004. A Note on the Relationship between Organic Solid Density and Liquid Density at the Triple Point. *Journal of Chemical & Engineering Data* 49, págs. 1512-1514.

Hermanto, M.W., Yeoh, A., Soh, B., Chow, P.S., Tan, R.B., 2015. Robust Crystallization Process Development for the Metastable δ -form of Pyrazinamide. *Organic Process Research & Development* 19, 1987-1996.

Hilfiker, R., 2006. *Polymorphism in the pharmaceutical industry.* Wiley Online Library.

Inès, G., Maria, B., Bernard, D., Josep-Lluís, T., René, C., Rietveld, I.B., 2013. Benzocaine polymorphism: pressure-temperature phase diagram involving forms II and III. *Int J Pharm* 456, 480-488.

Jarzembska, K.N., Hoser, A.A., Kamiński, R., Madsen, A.Ø., Durka, K., Woźniak, K., 2014. Combined experimental and computational studies of pyrazinamide and nicotinamide in the context of crystal engineering and thermodynamics. *Crystal Growth & Design* 14, 3453-3465.

Kulla, H., Greiser, S., Benemann, S., Rademann, K., Emmerling, F., 2016. In situ investigation of a self-accelerated cocrystal formation by grinding pyrazinamide with oxalic acid. *Molecules* 21, 917.

Kulla, H., Greiser, S., Benemann, S., Rademann, K., Emmerling, F., 2017. Knowing When To Stop · Trapping Metastable Polymorphs in Mechanochemical Reactions. *Crystal Growth & Design* 17, 1190-1196.

Lavor, E.P., Freire, F.D., Aragão, C.F.S., Raffin, F.N., 2012. Application of thermal analysis to the study of anti-tuberculosis drug compatibility. Part 1. *Journal of thermal analysis and calorimetry* 108, 207-212.

Liu, F., Song, Y., Liu, Y.-N., Li, Y.-T., Wu, Z.-Y., Yan, C.-W., 2018. Drug-bridge-drug ternary cocrystallization strategy for antituberculosis drugs combination. *Crystal Growth & Design* 18, 1283-1286.

Lourenço, C., Melo, C.I., Bogel-Łukasik, R., Bogel-Łukasik, E., 2012. Solubility Advantage of Pyrazine-2-carboxamide: Application of Alternative Solvents on the Way to the Future Pharmaceutical Development. *Journal of Chemical & Engineering Data* 57, 1525-1533.

Lourenço, C., Melo, C.I., Bogel-Łukasik, R., Bogel-Łukasik, E., 2012. Solubility advantage of pyrazine-2-carboxamide: application of alternative solvents on the way to the future pharmaceutical development. *Journal of Chemical & Engineering Data* 57, 1525-1533.

Luo, Y.-H., Liu, Q.-L., Yang, L.-J., Wang, W., Ling, Y., Sun, B.-W., 2015. Quantitative comparisons between α , β , γ , and δ pyrazinamide (PZA) polymorphs. *Research on Chemical Intermediates* 41, 7059-7072.

Luo, Y.-H., Sun, B.-W., 2013. Pharmaceutical Co-Crystals of Pyrazinecarboxamide (PZA) with Various Carboxylic Acids: Crystallography, Hirshfeld Surfaces, and Dissolution Study. *Cryst. Growth Des.* 13, 2098-2106.

Morris, K.R., Griesser, U.J., Eckhardt, C.J., Stowell, J.G., 2001. Theoretical approaches to physical transformations of active pharmaceutical ingredients during manufacturing processes. *Advanced drug delivery reviews* 48, 91-114.

Nakata, K., Takaki, Y., 1987. *Mem.Osaka Kyoiku Univ.Ser.* 3, 93.

Negoro, H., 1959. Solubility phenomena of pyridine-and pyrazinemonocarboxamides. I. Heat of sublimation of picolinamide, nicotinamide, isonicotinamide, and pyrazinecarboxamide. *Takamine Kenkyusho Nempo* 11, 66-75.

Negoro, H., Miki, T., Ueda, S., 1960. Solubility phenomena of pyridine- and pyrazinemonocarboxamides. I. Heat of sublimation of picolinamide, nicotinamide, isonicotinamide, and pyrazinecarboxamide. *Yakugaku Zasshi* 80, 665-669.

Pajula, K., Taskinen, M., Lehto, V.-P., Ketolainen, J., Korhonen, O., 2010. Predicting the formation and stability of amorphous small molecule binary mixtures from computationally determined Flory–Huggins interaction parameter and phase diagram. *Molecular pharmaceutics* 7, 795-804.

Rajalakshmi, G., Hathwar, V.R., Kumaradhas, P., 2014. Intermolecular interactions, charge - density distribution and the electrostatic properties of pyrazinamide anti - TB drug molecule: an experimental and theoretical charge - density study. *Acta Crystallographica Section B* 70, 568-579.

Rajbongshi, T., Sarmah, K.K., Sarkar, A., Ganduri, R., Cherukuvada, S., Thakur, T.S., Thakuria, R., 2018. Preparation of Pyrazinamide Eutectics versus Cocrystals Based on Supramolecular Synthons Variations. *Crystal Growth & Design* 18, 6640-6651.

Ribeiro da Silva, M.D., Miranda, M.S., Vaz, C.M., Matos, M.A.R., Acree Jr, W., 2005. Experimental thermochemical study of three monosubstituted pyrazines. *The Journal of Chemical Thermodynamics* 37, 49-53.

Rietveld, I.B., Barrio, M., Tamarit, J.L., Nicolai, B., Van de Streek, J., Mahé, N., Ceolin, R., Do, B., 2011. Dimorphism of the prodrug I - tyrosine ethyl ester: Pressure–temperature state diagram and crystal structure of phase II. *Journal of pharmaceutical sciences* 100, 4774-4782.

Rietveld, I.B., Barrio, M., Veglio, N., Espeau, P., Tamarit, J.L., Céolin, R., 2010. Temperature and composition-dependent properties of the two-component system D- and L-camphor at 'ordinary' pressure. *Thermochimica Acta* 511, 43-50.

Rø, G., Sørum, H., 1972a. The crystal and molecular structure of β - pyrazinecarboxamide. *Acta Crystallographica Section B* 28, 991-998.

Rø, G., Sørum, H., 1972b. The crystal and molecular structure of δ - pyrazinecarboxamide. *Acta Crystallographica Section B* 28, 1677-1684.

Rodriguez-Carvajal, J., Roisnel, T., Gonzales-Platas, J., 2005. FullProf suite (2005 version). CEA-CNRS, CEN Saclay, France: Laboratoire Léon Brillouin.

Sharma, P., Nandi, R., Gangopadhyay, D., Singh, A., Singh, R.K., 2018. Temperature dependent polymorphism of pyrazinamide: An in situ Raman and DFT study. *Spectrochimica Acta Part A: Molecular and Biomolecular Spectroscopy* 190, 177-180.

Smets, M., Baaklini, G., Tijink, A., Sweers, L., Vossen, C., Brandel, C., Meekes, H., Cuppen, H., Coquerel, G., 2018. Inhibition of the Vapor-Mediated Phase Transition of the High Temperature Form of Pyrazinamide. *Crystal growth & design* 18, 1109-1116.

Su, Y., Xu, J., Shi, Q., Yu, L., Cai, T., 2018. Polymorphism of griseofulvin: concomitant crystallization from the melt and a single crystal structure of a metastable polymorph with anomalously large thermal expansion. *Chemical Communications* 54, 358-361.

Takaki, Y., Sasada, Y., Watanabé, T., 1960. The crystal structure of α -pyrazinamide. *Acta Crystallographica* 13, 693-702.

Tamura, C., Kuwano, H., Sasada, Y., 1961. Crystallographic data of carboxylic acids and carboxyamides of picoline and pyrazine derivatives. *Acta Crystallographica* 14, 693-693.

Tan, X., Wang, K., Li, S., Yuan, H., Yan, T., Liu, J., Yang, K., Liu, B., Zou, G., Zou, B., 2012. Exploration of the pyrazinamide polymorphism at high pressure. *The Journal of Physical Chemistry B* 116, 14441-14450.

Thakuria, R., Cherukuvada, S., Nangia, A., 2012. Crystal Structures of Pyrogallol, Its Hydrate, and Stable Multiple Z' Cocrystals with N-Heterocycles Containing Metastable Conformers of Pyrogallol. *Crystal Growth & Design* 12, 3944-3953.

Tiwari, R.K., Deo, N., Singh, T.P., 1980. *J. Sci. Res. Bhopal, India* 2, 161.

Tiwari, R.K., Patel, T.C., Singh, T.P., 1982. *Indian J. Phys. Sect. A* 56, 413.

Toscani, S., Céolin, R., Ter Minassian, L., Barrio, M., Veglio, N., Tamarit, J.-L., Louër, D., Rietveld, I.B., 2016. Stability hierarchy between Piracetam forms I, II, and III from experimental pressure–temperature diagrams and topological inferences. *International journal of pharmaceutics* 497, 96-105.

Wahlberg, N., Ciochoń, P., Petriček, V., Madsen, A.Ø., 2013. Polymorph stability prediction: on the importance of accurate structures: a case study of pyrazinamide. *Crystal Growth & Design* 14, 381-388.

Wang, J.-R., Ye, C., Mei, X., 2014. Structural and physicochemical aspects of hydrochlorothiazide co-crystals. *CrystEngComm* 16, 6996-7003.

Wheate, N.J., Vora, V., Anthony, N.G., McInnes, F.J., 2010. Host-guest complexes of the antituberculosis drugs pyrazinamide and isoniazid with cucurbit [7] uril. *Journal of Inclusion Phenomena and Macrocyclic Chemistry* 68, 359-367.

Würlinger, A., 1975. Differential thermal analysis under high pressure IV: Low - temperature DTA of solid - solid and solid - liquid transitions of several hydrocarbons up to 3 kbar. *Berichte der Bunsengesellschaft für physikalische Chemie* 79, 1195-1201.

Zhang, K., Shen, H., Xu, S., Zhang, H., Zhu, M., Shi, P., Fu, X., Yang, Y., Gong, J., 2017. Thermodynamic study of solubility for pyrazinamide in ten solvents from T=(283.15 to 323.15) K. *The Journal of Chemical Thermodynamics* 112, 204-212.

Figure Captions

Figure 1. Molecular structure of pyrazinamide, molecular weight M is $123.11 \text{ g mol}^{-1}$

Figure 2. DSC curve (10 K min^{-1}) of commercial pyrazinamide form α transforming into γ at around 425 K , which melts at around 462 K (black line) and a DSC curve of a sample with a very large specific volume ($V_{\text{pan}}/m_{\text{PZA}}$) of which only the end of sublimation can be observed (449 K , red line). **Inset:** a close-up of the DSC curve of 0.01 mg illustrating the end of sublimation before the melting point of γ is reached. The extension of the baseline is indicated by the blue dotted line.

Figure 3. The enthalpy of fusion of form γ as a function of the specific volume available to PZA in the DSC capsule (see text). **Inset:** close-up on the evolution of the enthalpy of fusion at low specific volume. An upward curvature of the line at low specific volume can be observed.

Figure 4. Transition temperature of the α to γ transition obtained by DSC at different heating rates. No conclusive equilibrium temperature can be obtained from this behavior (equilibrium temperature from Table 4 indicated for reference).

Figure 5. (a) High-pressure differential thermal analysis curves, **(b)** The transition pressure of α to γ (■) and the melting pressure of γ (●) as a function of the temperature.

Figure 6. The X-ray diffraction patterns of pyrazinamide **(a)** form α and **(b)** form γ at different temperatures ($\lambda = 1.54056 \text{ \AA}$).

Figure 7. The specific volume of pyrazinamide form α and form γ at different temperatures. (■) α form this work, (●) γ form this work, (□) α form from the literature (A.Nangia and A.Srinivasulu, 2005; Battilocchio et al., 2014; Rajalakshmi et al., 2014; Takaki et al., 1960; Tiwari et al., 1980; Tiwari et al., 1982), (○) γ form from the literature (Castro et al., 2009; Cherukuvada et al., 2010; Nakata and Takaki, 1987; Tamura et al., 1961). The error bars for the data obtained in this work are smaller than the symbols.

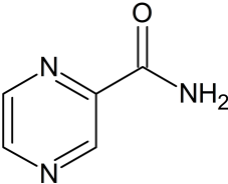
Figure 8. The specific volumes of polymorphs α and γ as a function of pressure. (■) α form, (●) γ form at 295 K . The error bars are smaller than the symbols.

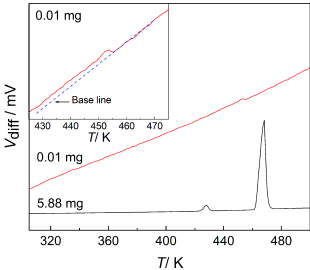
Figure 9. The solubility of polymorphs α and γ at different temperatures. (■) α (this work), (●) γ (this work), (▲) α obtained by Hermanto et al., (◆) α obtained by Zhang et al. (▼) γ

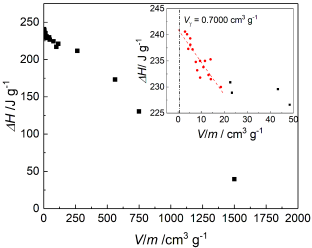
obtained by Hermanto et al. The error bars for the data obtained in this work are smaller than the symbols.

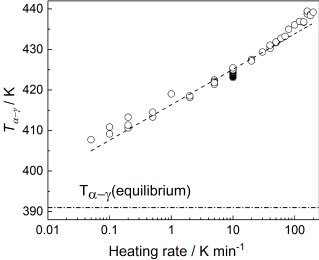
Figure 10. A sketch of the thermal expansion of the liquid in relation to the thermal expansion of the solids.

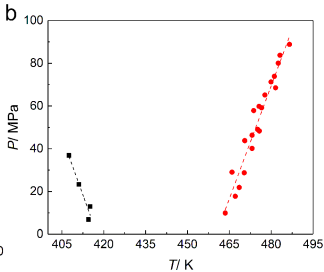
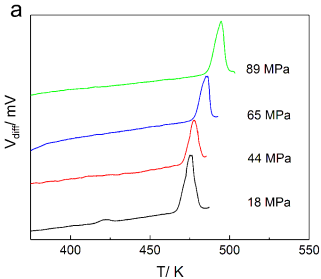
Figure 11. The two-panel pressure-temperature phase diagram of the α and γ polymorphs, the liquid, L, and the vapor phase, V. **High pressure panel (Top):** Two-phase equilibria: black (line + points (■)): α - γ , blue line: α -L, red (line + points (■)): γ -L. (●) is metastable triple point α - γ -L, (●) is stable triple point α - γ -V, (●) is metastable triple point α -L-V and (●) is stable triple point γ -L-V. **Low pressure panel (below):** Zoom on the vapor phase with orange line: L-V equilibrium, purple line: γ -L equilibrium and green line α -L equilibrium. Solid lines: stable equilibria, dashed lines: metastable equilibria, dotted lines: super-metastable equilibria. Solid circle: stable triple point, semi-solid circle: metastable triple point.

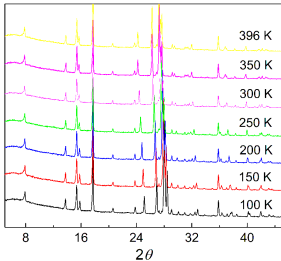










a**b**